

## RESEARCH ARTICLE

# Systematic expression profiling of Dpr and DIP genes reveals cell surface codes in *Drosophila* larval motor and sensory neurons

Yupu Wang<sup>1,2,3</sup>, Meike Lobb-Rabe<sup>1,2,4</sup>, James Ashley<sup>1,2</sup>, Purujit Chatterjee<sup>1,2</sup>, Veera Anand<sup>1,2</sup>, Hugo J. Bellen<sup>5,6</sup>, Oguz Kanca<sup>5</sup> and Robert A. Carrillo<sup>1,2,3,4,\*</sup>

## ABSTRACT

In complex nervous systems, neurons must identify their correct partners to form synaptic connections. The prevailing model to ensure correct recognition posits that cell-surface proteins (CSPs) in individual neurons act as identification tags. Thus, knowing what cells express which CSPs would provide insights into neural development, synaptic connectivity, and nervous system evolution. Here, we investigated expression of Dpr and DIP genes, two CSP subfamilies belonging to the immunoglobulin superfamily, in *Drosophila* larval motor neurons (MNs), muscles, glia and sensory neurons (SNs) using a collection of GAL4 driver lines. We found that Dpr genes are more broadly expressed than DIP genes in MNs and SNs, and each examined neuron expresses a unique combination of Dpr and DIP genes. Interestingly, many Dpr and DIP genes are not robustly expressed, but are found instead in gradient and temporal expression patterns. In addition, the unique expression patterns of Dpr and DIP genes revealed three uncharacterized MNs. This study sets the stage for exploring the functions of Dpr and DIP genes in *Drosophila* MNs and SNs and provides genetic access to subsets of neurons.

**KEY WORDS:** Dpr, DIP, Motor neuron, Sensory neuron, Synaptic recognition

## INTRODUCTION

During nervous system development, neurons contact thousands of cells but only form synapses with a small subset. Precise neural wiring is achieved through a series of steps, including axon pathfinding, partner recognition and synaptic pruning (Sanes and Zipursky, 2020; Zarin and Labrador, 2019). Although the mechanisms underlying these processes are not completely understood, one prevailing model proposes that cell-surface proteins (CSPs) instruct chemoattraction and -repulsion, self-avoidance, and synaptic partner recognition (Honig and Shapiro,


2020; Wit and Ghosh, 2016). CSPs fall into several protein families, including the immunoglobulin superfamily (IgSF), the cadherin protein family (Cdhs), the leucine-rich repeat protein family (LRRs), the receptor tyrosine kinases (RTKs) and many more (Bali et al., 2022; Jontes, 2017; Kurusu et al., 2008; Sanes and Zipursky, 2020; Zinn and Özkan, 2017). *In vitro* biochemical studies have shown that subsets of these CSPs interact in a homo- or heterophilic manner, and many of these interactions are implicated in synaptic connectivity in both vertebrates and invertebrates (Cheng et al., 2019; Honig and Shapiro, 2020; Özkan et al., 2013; Wit and Ghosh, 2016).

The genetically tractable *Drosophila melanogaster* is an excellent model in which to study CSP expression and function owing to its stereotyped neurogenesis and circuit wiring as well as the availability of an extensive range of genetic tools. Neurons in the fly brain assemble into highly complex circuits similar to those observed in vertebrates but numerically less daunting. In the fly mushroom body, neurons rely on different isoforms of Dscam1 to discriminate self from non-self (Hattori et al., 2009; Wang et al., 2004; Zhan et al., 2004). In the olfactory system, the epidermal growth factor (EGF) repeat-containing transmembrane Teneurin proteins Ten-m and Ten-a are required for the one-to-one matching between olfactory receptor neurons and projection neurons (Hong et al., 2012).

Specific challenges are also encountered in the *Drosophila* embryonic/larval neuromuscular system; 33 motor neurons (MNs) within each neuromere in the ventral nerve cord (VNC) send their projections to the periphery where they follow defined paths and ultimately choose specific muscle(s) to innervate among 30 potential targets (Grueber et al., 2007; Hoang and Chiba, 2001; Menon et al., 2013). Each efferent motor neuron can be recognized by its stereotypical innervation pattern and morphology. Utilizing the neuromuscular system, many CSPs have been identified as recognition cues between MNs and muscles, including Toll proteins (Inaki et al., 2010; Rose et al., 1997), Connectin (Nose et al., 1992, 1997) and Capricious (Kurusu et al., 2008; Shishido et al., 1998) from the LRR family, and Fasciclin 2 (Davis et al., 1997; Winberg et al., 1998) and Fasciclin 3 (Chiba et al., 1995; Kose et al., 1997) from the IgSF. In contrast, the afferent neurons of the sensory nervous system are localized in the periphery and send their projections to the VNC. Forty-two sensory neurons (SNs) are stereotypically distributed throughout each hemisegment of the larval body wall and establish synaptic connections with interneurons (Orgogozo and Grueber, 2005). Studies from dendritic arborization (da) neurons identified several CSPs that are required for self-avoidance, such as Dscam1 and semaphorin proteins (Meltzer et al., 2016; Miura et al., 2013; Soba et al., 2007). Thus, the unambiguous identification of cells in the motor and sensory circuits provides an ideal system in which to examine the genes and mechanisms that underlie synaptic specificity and development.

<sup>1</sup>Department of Molecular Genetics & Cellular Biology, University of Chicago, Chicago, IL 60637, USA. <sup>2</sup>Neuroscience Institute, University of Chicago, Chicago, IL 60637, USA. <sup>3</sup>Committee on Development, Regeneration, and Stem Cell Biology, University of Chicago, Chicago, IL 60637, USA. <sup>4</sup>Program in Cell and Molecular Biology, University of Chicago, Chicago, IL 60637, USA. <sup>5</sup>Department of Molecular and Human Genetics and Jan and Dan Duncan Neurobiological Research Institute, Baylor College of Medicine (BCM), Houston, TX 77030, USA. <sup>6</sup>Department of Neuroscience and Howard Hughes Medical Institute, Baylor College of Medicine (BCM), Houston, TX 77030, USA.

\*Author for correspondence (robertcarrillo@uchicago.edu)

 Y.W., 0000-0002-3553-0680; M.L.-R., 0000-0001-6486-7752; J.A., 0000-0002-6693-1014; H.J.B., 0000-0001-5992-5989; O.K., 0000-0001-5438-0879; R.A.C., 0000-0002-2067-9861

In a previous ‘interactome’ screen, we and others identified two subfamilies of the *Drosophila* IgSF, the Defective proboscis response proteins (Dprs; 21 members) and the Dpr-interacting proteins (DIPs; 11 members) (Carrillo et al., 2015; Özkan et al., 2013). Dprs and DIPs provide a vast repertoire of unique combinations for synaptic specificity. Interactions between Dprs and DIPs have been implicated in synaptic connectivity, cell survival and synaptic growth (Ashley et al., 2019; Bornstein et al., 2021; Carrillo et al., 2015; Courgeon and Desplan, 2019; Menon et al., 2019; Sanes and Zipursky, 2020; Venkatasubramanian et al., 2019; Xu et al., 2018, 2019). However, most studies focused on Dprs and DIPs have implicated only a small subset, likely due to low-penetrance targeting defects and molecular redundancy. For example, in the larval neuromuscular circuit, loss of *DIP-α* leads to complete loss of muscle 4 innervation by a specific motor neuron; however, most neuromuscular junctions (NMJs) on other muscles formed by the same neuron are unaffected, suggesting that different synaptic recognitions utilize different pairs of CSPs even within the same neuron (Ashley et al., 2019). Thus, obtaining a complete expression map of families of CSPs in individual neurons within specific circuits would facilitate subsequent functional studies.

In this study, we interrogate the expression patterns of Dpr and DIP genes. We generated a collection of GAL4 lines and utilized different UAS reporters to examine expression of Dpr and DIP genes in *Drosophila* larval neuromuscular and sensory circuits. We showed expression maps of Dpr and DIP genes in MNs, SNs and muscles, and found that each MN and SN expresses a unique subset of Dpr and DIP genes. Utilizing hierarchical clustering, we found that the same class of SNs expresses similar Dpr and DIP genes, suggesting roles in identifying overlapping synaptic partners. Finally, the highly distinct expression patterns of Dpr and DIP genes in MNs revealed previously unidentified MNs. The expression analyses generated by this study will benefit future functional studies of Dprs and DIPs in the motor and sensory circuits. The genetic tools and pipeline provided here will facilitate expression studies of Dprs and DIPs, and other CSPs, in other *Drosophila* neural circuits to promote the discovery of identification tags utilized for circuit assembly.

## RESULTS

### Generating a GAL4 collection of Dpr and DIP genes

Using *Drosophila* Minos-mediated integration cassette (MiMIC) insertions followed by Trojan conversion, and CRISPR-mediated integration cassette (CRIMIC) insertions, we and others generated a collection of GAL4 lines of all DIP genes and *dpr1-dpr19* (Diao et al., 2015; Kanca et al., 2019; Lee et al., 2018; Nagarkar-Jaiswal et al., 2015a; Venken et al., 2011) (Fig. 1A). For each *dpr*- and *DIP-GAL4*, the cassette is inserted into a common intron or the 5'UTR shared by all isoforms (Fig. 1A, Table S1). Therefore, GAL4 should report the expression of all isoforms of each gene. Insertion of the *SA-T2A-GAL4-PolyA* should generate truncated transcripts because of the presence of the PolyA tail (Logan et al., 1987; Zhang et al., 2015). In addition, the presence of a T2A-*GAL4* leads to an arrest during translation at the T2A site followed by a re-initiation of translation at the GAL4 sequence (Diao et al., 2015; Szymczak-Workman et al., 2012). To confirm the disruption of the gene of interest, we measured transcript expression by qRT-PCR using primers downstream of the insertion site and confirmed that most GAL4 lines are loss-of-function alleles. For example, in homozygous viable GAL4 lines, *DIP-α-GAL4* and *DIP-ζ-GAL4* showed no detectable *DIP-α* and *DIP-ζ* mRNA, respectively (Fig. S1A), suggesting they are null alleles. Several GAL4 lines,

such as *DIP-β-GAL4* and *dpr15-GAL4*, showed a reduction in mRNA levels, whereas some lines, such as *DIP-τ-GAL4* and *dpr16-GAL4*, showed no change in mRNA expression. Although these GAL4 lines do not show a significant loss of transcription, the T2A sequence should still disrupt translation and generate mutant proteins. For homozygous lethal lines, we examined mRNA levels in heterozygous animals and found that most GAL4 lines show expression near 50% (Fig. S1B), suggesting these GAL4 lines are severe loss-of-function alleles. The qRT-PCR results are summarized in Table S2. In summary, approximately 70% of the insertions caused a severe disruption of transcription.

Because most GAL4 insertions are mutants, we used heterozygotes to map Dpr and DIP gene expression. Loss of a single copy of any Dpr and DIP gene did not affect gross viability, cell survival or synaptic connectivity in heterozygotes as revealed by presence of a postsynaptic marker, Discs Large (DLG), and a presynaptic marker, anti-horseradish peroxidase (HRP; a marker for all neuronal membranes; Jan and Jan, 1982) (see Materials and Methods). Thus, the *dpr/DIP-GAL4* driver lines should faithfully report the cells that express Dpr and DIP genes (Lee et al., 2018; Nagarkar-Jaiswal et al., 2015b).

### Expression of Dpr and DIP genes in MNs

The larval body wall is segmented, and each abdominal hemisegment consists of 30 muscles that are grouped into three major muscle groups: ventral, lateral and dorsal (Fig. 1B) (Bate, 1990; Hooper, 1986; Zarin et al., 2019). Innervating those muscles are 33 MNs classified as type-I (29), type-II (3) and type-III (1) based on their terminal morphology and neurotransmitter type (Choi et al., 2004; Hoang and Chiba, 2001; Landgraf et al., 1997; Zarin et al., 2019). All MN axon terminals contain strings of bead-like structures called boutons which house the active zones. Type-I MNs are excitatory glutamatergic neurons, and they are further subdivided into type-I big (Ib) and type-I small (Is) based on their bouton size and innervation patterns: Ib MNs (in the larva named MN1-Ib to MN30-Ib corresponding to the muscle number) generally have larger boutons and innervate single muscle fibers whereas Is MNs have smaller boutons and innervate muscle groups (Choi et al., 2004; Lnenicka and Keshishian, 2000). The Is MN that innervates ventral muscles is referred to as the ventral common exciter (vCE), RP5 or MNISNb/d-Is, and the Is MN that innervates dorsal muscles is called the dorsal common exciter (dCE), RP2 or MNISN-Is (Broadus et al., 1995; Doe et al., 1988; Takizawa et al., 2007). Similarly, three neuromodulatory type-II MNs innervate the ventral, lateral and dorsal muscle groups, and the single type-III MN primarily innervates m12 (Hoang and Chiba, 2001; Schmid et al., 1999). Based on these distinguishing features – terminal morphology and innervation patterns – we can unambiguously identify MNs that express each Dpr and DIP gene.

To examine the expression of Dpr and DIP genes in MNs, we first crossed each GAL4 line to a fluorescent reporter line and monitored reporter expression at third instar NMJs (Fig. 2A). GAL4 lines derived from MiMIC insertions were crossed to a GFP reporter, whereas CRIMIC GAL4 lines were crossed to an mCherry reporter as CRIMIC insertions carry a 3XP3-GFP marker that expresses in glial cells and the lateral bipolar dendrite (lbd) neuron (Fig. S2). To identify all NMJs, we labeled preparations with antibodies against DLG and HRP and confirmed that the gross muscle innervation was normal in *dpr/DIP-GAL4* heterozygous lines. GFP or RFP labeling of NMJs revealed the corresponding MNs that express each Dpr and DIP gene. We followed this pipeline for each *dpr/DIP-GAL4* to record expression in all MNs.

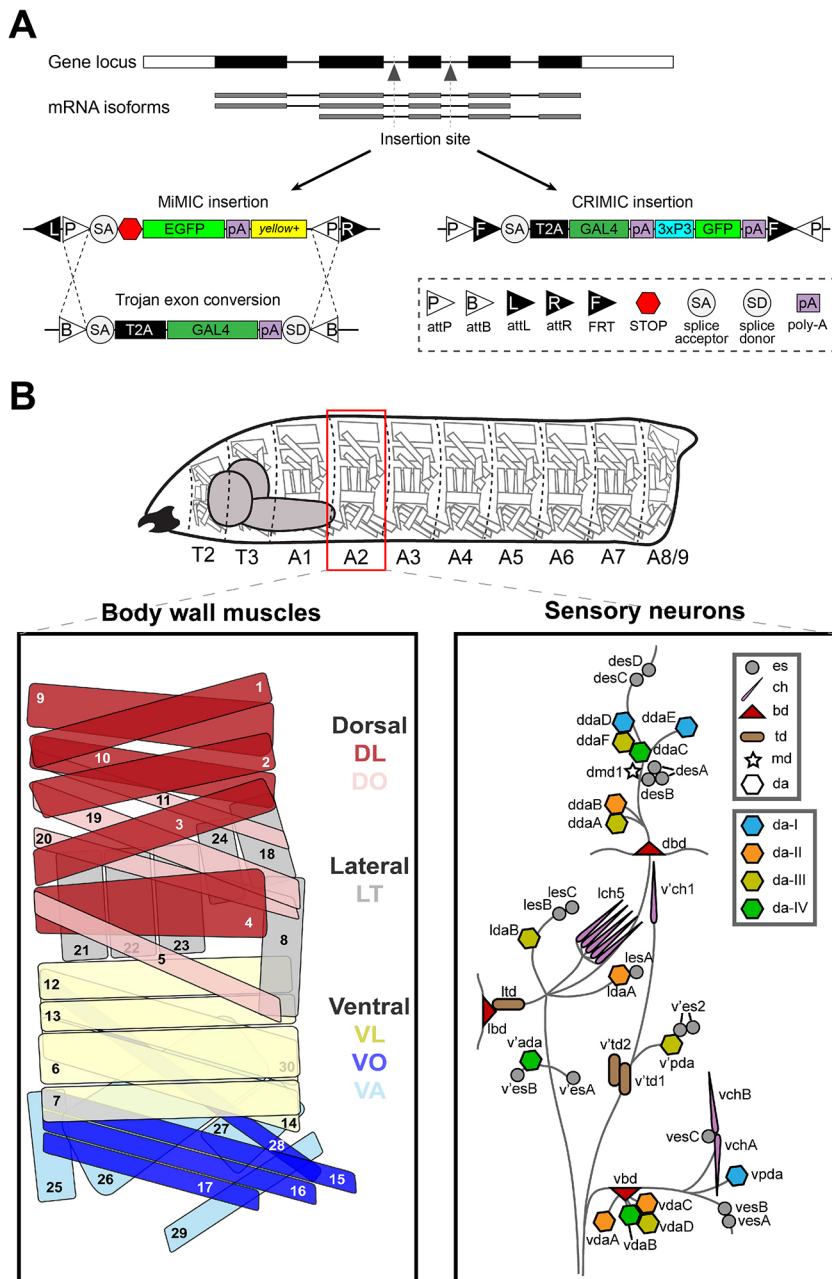


**Fig. 1. Schematic of GAL4 insertion and larval body plan.** (A) MiMIC or CRIMIC cassettes were inserted into a common intron or 5'UTR to capture the expression of all isoforms for each Dpr and DIP gene. MiMIC insertions were flanked by two attP sites which are later swapped by a GAL4 exon or T2A-GAL4 trojan exon. (B) *Drosophila* larvae are divided into three thoracic segments and nine abdominal segments, with repeated muscles, MNs and SNs. Muscles are divided into three main groups, the ventral, lateral and dorsal muscles. MNs innervating these muscles are not shown in this diagram. SNs are divided into six main classes: the es neurons, ch neurons, bd neurons, td neurons, md neuron and da neurons (Orgogozo and Grueber, 2005). In addition, da neurons are further divided into da-I, da-II, da-III and da-IV subclasses.

We first confirmed some previously observed expression patterns (Ashley et al., 2019; Carrillo et al., 2015); for example, *DIP- $\alpha$*  was selectively expressed in Is MNs but not in Ib MNs (Fig. S3A). Interestingly, we found that several Dpr and DIP genes are not always expressed at the same level in a specific MN. For example, *DIP- $\delta$ -GAL4* only labeled 22% of MN12-Ib (ten out of 45 MN12-Ib examined; Fig. S3B). Similarly, *dpr16-GAL4* was expressed in ten out of 25 MN30-Ib and nine out of 25 MN14-Ib examined. In addition to Ib and Is MNs, we also revealed expression in type-II and type-III MNs. For example, *dpr16-GAL4* was expressed in type-II MNs but not the type-III MN (Fig. S4A,B), whereas *DIP- $\kappa$ -GAL4* was expressed in the type-III MN but not in type-II MNs (Fig. S4C,D). Surprisingly, we also found that some Dpr and DIP genes are expressed in a gradient along the anterior to posterior axis. For example, *dpr2* showed high expression in MN1-Ib in the anterior but became undetectable from abdominal segment 4 (A4) to the posterior (Fig. 2B). *DIP- $\zeta$ -GAL4*, by contrast, labeled anterior

MN16/17-Ib weakly, but was much stronger in the posterior (Fig. 2C). These complex expression patterns suggest intricate regulatory mechanisms of Dpr and DIP genes.

Work from our lab and others suggested that Dprs and DIPs are synaptic recognition molecules. In the fly neuromuscular circuit, MN axons explore the musculature field beginning at embryonic stage 14 and synaptic markers are observed at stage 16 (Yoshihara et al., 1997). A regular UAS reporter will only report real-time expression and will not reveal if a Dpr or DIP gene is temporally expressed earlier in development. To capture the temporal expression patterns of Dpr and DIP genes, we utilized a permanent labeling reporter to constantly label the GAL4-expressing neuron (Fig. 2A). Interestingly, we observed only a few Dpr and DIP genes that are temporally expressed in MNs. For example, MN21/22-Ib is not labeled when *dpr9-GAL4* is crossed to *UAS-GFP*, but with the permanent labeling reporter, the same neuron showed strong expression (Fig. 2D). The temporal



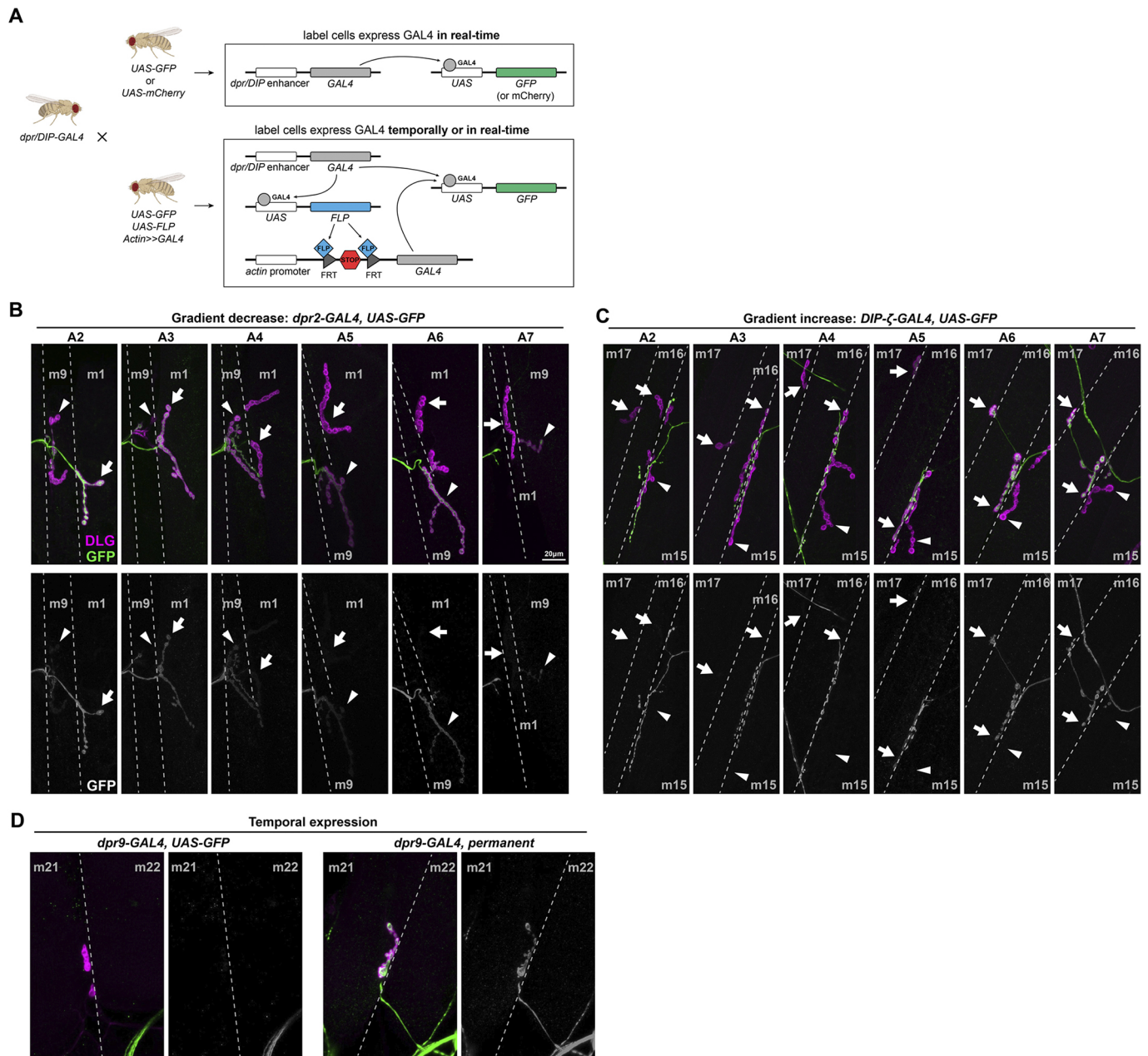


**Fig. 2. Dpr and DIP genes are expressed in various patterns in MNs.** (A) Schematic showing the experimental procedure. Each *dpr/DIP-GAL4* line was crossed to a real-time reporter (*UAS-GFP* or *UAS-mCherry*) and a permanent reporter [*UAS-GFP, UAS-FLP, actin-(FRT.STOP)-GAL4*] to reveal the dynamic expression of Dpr and DIP genes. (B) Example of a decrease in expression of *dpr2-GAL4* in MN1-lb (arrows) from anterior hemisegment A2 to posterior hemisegment A7. Note that the expression in nearby MN9-lb (arrowheads) is also not robust as it was not expressed in A2 and A3 but was expressed in A4 to A7. (C) Example of an increase in expression of *DIP-ζ-GAL4* in MN16/17-lb (arrows) from anterior hemisegment A2 to posterior hemisegment A7. Note that the expression in nearby MN15/16-lb (arrowheads) was always absent. (D) Example of temporal expression of *dpr9-GAL4* in MN21-lb. MN21-lb was not labeled by *dpr9-GAL4>GFP* animals, but 50% of MN21-lb were labeled in the cross to the permanent reporter. Dashed lines indicate muscle boundaries.

expression of only a small subset of Dpr and DIP genes suggests that most of these CSPs may function in different steps of nervous system development. It is noteworthy that the CRIMIC cassettes are excisable by Flippase as well due to the presence of flanking FRT sites (Fig. 1A). However, because of the activation of the permanent *actin-GAL4*, the excision of CRIMIC cassettes does not pose a technical issue.

The expression of Dpr and DIP genes in all MNs is summarized in Fig. 3. Here, we included variable expression patterns (defined by

how frequently a cell expresses the reporter) and gradient and temporal expression patterns. Criteria for each expression category is described in Materials and Methods and in Fig. S5. In general, Dpr genes are expressed in many MNs whereas DIP genes are expressed much more selectively. Each MN expresses at least one DIP gene, and, overall, each MN has a unique Dpr and DIP gene expression signature. Taken together, we generated an expression map of Dpr and DIP genes in all larval MNs and found that each MN expresses a unique subset.



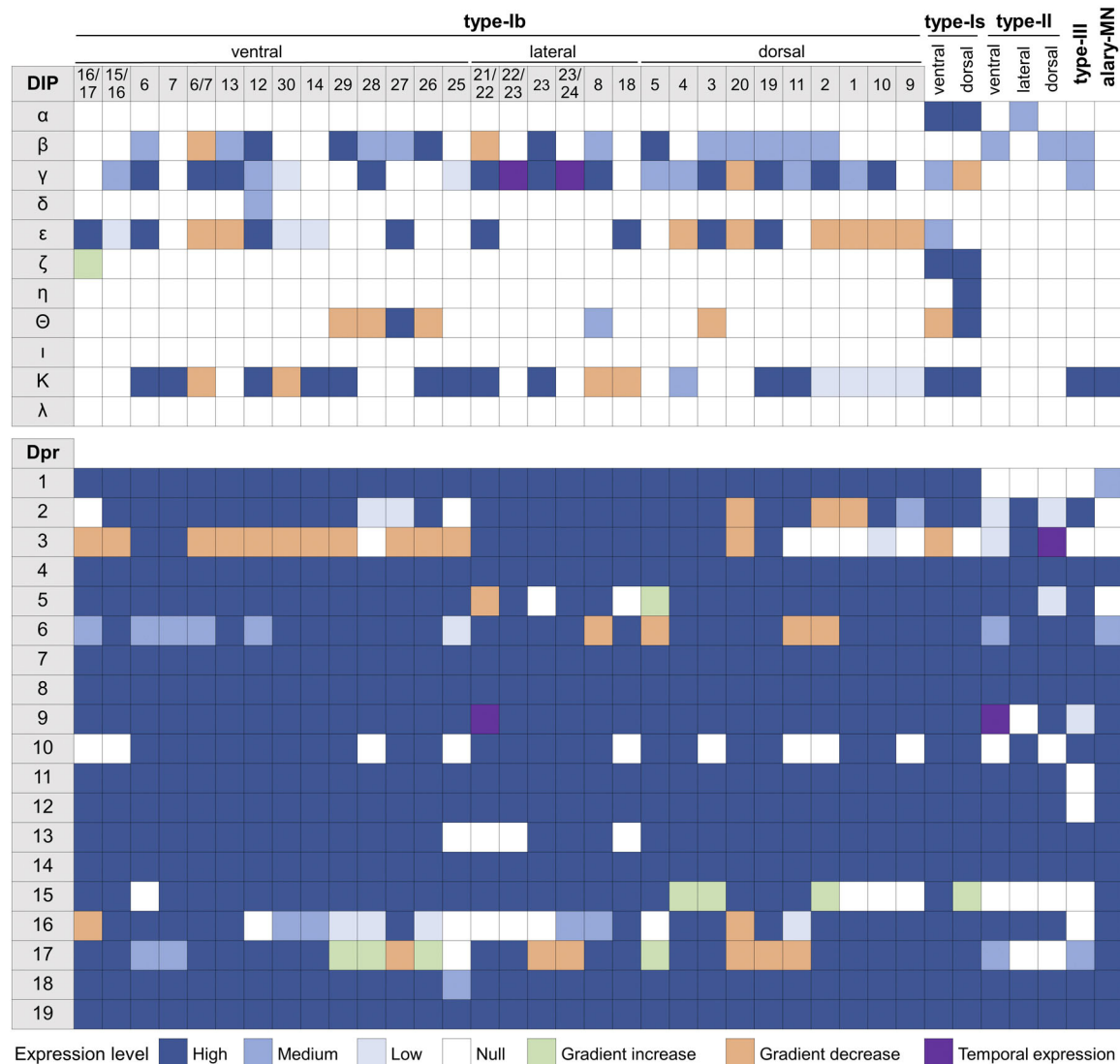


**Fig. 3. Expression map of Dpr and DIP genes in all larval MNs.** Each column represents an MN including type-Ib, type-Is, type-II, type-III and the alary MN. Expression of each gene in each MN is characterized into a specific category as indicated in the key. Note that MN16/17-Ib was named as MN15/16/17-Ib by Hoang and Chiba (2001); MN6-Ib is represented only in A2 hemisegments (see further characterization below); MN7-Ib is represented only in A2 hemisegments (see further characterization below); and MN23-Ib is a newly identified neuron (see further characterization below).

### Expression of Dpr and DIP genes in muscles

In a previous study, we observed *dpr10* expression in ventral and dorsal muscles and its interacting partner, *DIP-α*, in Is MNs (Ashley et al., 2019). To label muscle nuclei and report both temporal and real-time gene expression, we used the G-TRACE system (Evans et al., 2009), which takes advantage of FLP-FRT and GAL4/UAS (Fig. 4A). If a GAL4 is transiently expressed, then cell nuclei will be GFP positive. However, if the cell nuclei are labeled by both GFP and RFP, this may suggest the GAL4 is consistently expressed. We utilized the G-TRACE system and confirmed expression of *dpr10* in all longitudinal muscles, but not in oblique or transverse muscles (Fig. 4B,C). This expression pattern suggests distinct transcriptional regulation programs between muscle groups (Bate, 1990). In addition, we found that a small subset of muscles, such as m5 and m8, showed inconsistent expression of *dpr10* (Fig. 4B, arrow). Also, all muscle nuclei co-labeled with GFP and RFP in *dpr10-GAL4>G-TRACE*, suggesting that *dpr10* expression is maintained throughout larval development.

We examined other Dpr and DIP genes and found that *dpr19* is expressed in all muscles (Fig. 4D), including the oblique and transverse muscles (Fig. 4E). Unlike *dpr10*, most muscle nuclei in *dpr19-GAL4>G-TRACE* were only GFP positive, suggesting that *dpr19* is temporally expressed and turned off in late larval stages. To confirm this temporal expression, we examined *dpr19-GAL4>mCherry* first instar larva and observed a high level of muscle expression, which we did not observe in third instar (Fig. S6). Taken together, we showed that muscles express many fewer Dpr and DIP genes compared with motor and sensory neurons (Fig. 4F). These results suggest that a subset of Dpr and DIP genes may function in MN-muscle recognition and others in premotor neuron-MN recognition.

### Expression of Dpr and DIP genes in glial cells

In the *Drosophila* larval peripheral nervous system, glia play important roles in nervous system development and extensively interact with MN axons (Kottmeier et al., 2020). Therefore, we examined the glial expression of Dpr and DIP genes.

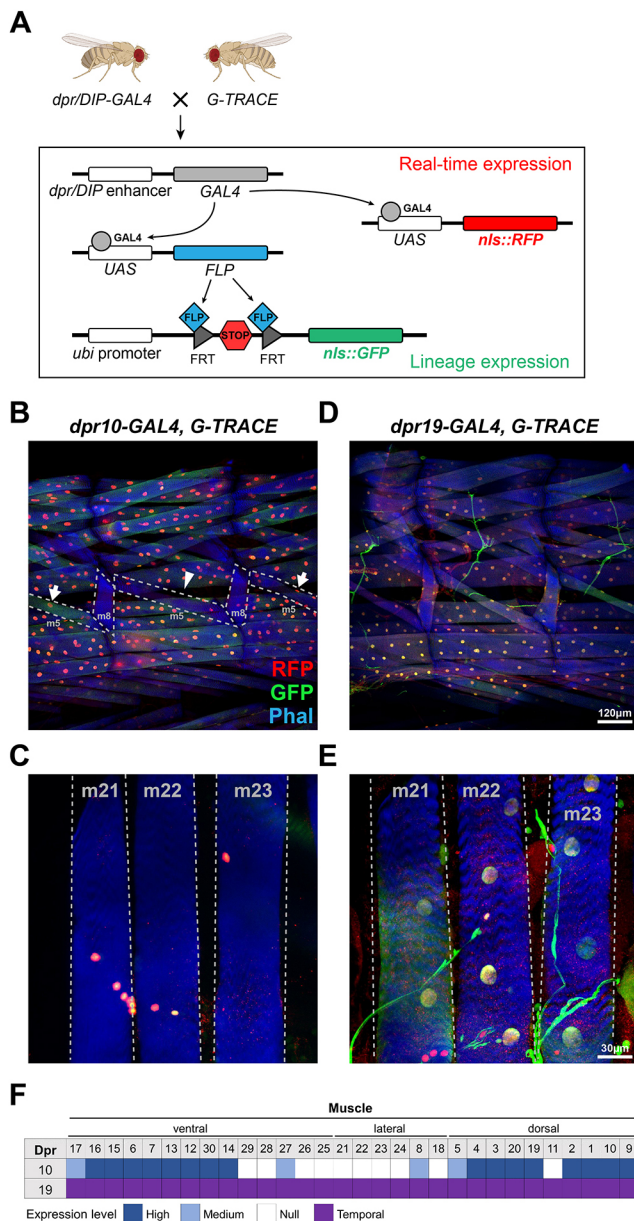


**Fig. 4. Using the G-TRACE system to probe expression of Dpr and DIP genes in muscles and glial cells.** (A) Schematic showing the cross between *dpr/DIP-GAL4* and the *G-TRACE* reporter. Red signal represents real-time GAL4 expression and green signal represents earlier GAL4 expression. (B,C) *dpr10* is consistently expressed in most muscles (B) but absent in transverse muscles (C) and some deeper ventral muscles. Expression in some muscles is not consistent. For example, in some hemisegments m5 nuclei are not labeled (arrowhead), but an adjacent hemisegment shows labeling of m5 nuclei (arrows). *dpr10* expression is maintained throughout development as revealed by co-labeling with GFP and RFP. (D,E) *dpr19* is expressed in all muscles (D), including transverse muscles (E). Compared with *dpr10*, these nuclei have less RFP intensity, which may indicate that *dpr19* is temporally expressed in early development and turned off later. (F) Expression map of *dpr10* and *dpr19* in muscles.

To distinguish glial and neuronal expression unambiguously, we used G-TRACE to probe glial expression. We crossed each *dpr/DIP-GAL4* line to the G-TRACE reporter and found that *dpr1* is expressed in glia (Fig. S7). Additionally, *dpr1* expression is highly dynamic as some glia temporarily express *dpr1* whereas others maintain *dpr1* expression. This result suggests that Dpr1 in glia and

its interacting partners DIP- $\eta$ , DIP- $\theta$  and DIP- $\iota$  in MNs (Fig. 3) may be involved in glia-neuron interactions to guide various processes, including neuronal development, axon pathfinding and synaptic homeostasis (Bittern et al., 2020; Yildirim et al., 2019).

### Expression of Dpr and DIP genes in SNs

Next, we examined expression of Dpr and DIP genes in larval SNs using a similar approach to the MN analyses. Two morphologically distinct types of SNs can be classified in the larval body wall (Fig. 1B) (Orgogozo and Grueber, 2005; Veling et al., 2019). Type-I SNs project a single dendrite that associates with chordotonal (ch) organs or external sensory (es) organs to detect mechanical and chemical stimuli. Type-II SNs are multidendritic (md) neurons that transmit proprioceptive information. Type-II SNs can be further classified into bipolar dendrite (bd) neurons, tracheal dendrite (td) neurons and da neurons. The da neurons are then subdivided into four classes based on the complexity of their dendrite morphology (da-I, da-II, da-III and da-IV) (Fig. 1B) (Grueber et al., 2002).

To examine expression of Dpr and DIP genes in SNs, we labeled larvae with anti-HRP to locate the cell bodies of SNs. The Dpr and DIP gene expression map in all SNs is shown in Fig. 5. Similar to MNs, DIP genes are more sparsely expressed in SNs compared with Dpr genes, which are broadly expressed. However, several Dpr genes (*dpr14*, *dpr15* and *dpr17*) are only expressed in a subset of SNs, unlike their broad expression pattern in MNs. We also observed that some Dpr and DIP genes are temporally expressed. For example, the dorsal da neurons (ddaA, -C, -F and -D) are labeled when *dpr5-GAL4* is crossed to the permanent labeling reporter, but not in *dpr5-GAL4*>*UAS-GFP* animals (Fig. S8). Taken together, we generated expression data for Dpr and DIP genes in SNs (Fig. 5) and showed that each SN expresses a unique subset of Dpr and DIP genes, providing support for their roles as identification tags.

### SNs in the same class express similar subsets of Dpr and DIP genes

Larval SNs can be divided into types based on their morphology and function, including ch, es, bd, td and da neurons. Although SNs from the same type are distributed throughout the body wall and project their afferent axons through different trajectories, their axon terminals innervate the same region in the VNC and contact common interneuron partners (Grueber et al., 2007; Landgraf et al., 2003a; Merritt and Murphey, 1992; Murphey et al., 1989). For example, the ventral, ventral' and lateral mechanosensory ch neurons all project to the ventral medial region of the VNC and share synapses with some interneurons (Heckscher et al., 2015; Valdes-Aleman et al., 2021). Similarly, different classes of da neurons innervate unique sections of the VNC (Grueber et al., 2007; Merritt and Whittington, 1995; Schrader and Merritt, 2000). Overall, these innervation patterns suggest that SNs from the same class may share similar identification tags to wire with common interneurons.

Dprs and DIPs have been implicated in synaptic partner recognition so we hypothesized that shared Dpr and DIP gene expression may be utilized by the same type/class of neurons to instruct connectivity. To test this model, we generated an unbiased hierarchical clustering of SNs based on their Dpr and DIP gene expression (Fig. 6A). Surprisingly, we found a high correlation between SN types/classes and expression of Dpr and DIP genes. For example, most es neurons are grouped together, as well as all ch neurons, indicating that these two subclasses of type-I SNs can be distinguished by their expression of Dpr and DIP genes. Similarly, subclasses of da neurons are clustered separately. We found that da-I neurons are identifiable by expression of *DIP- $\theta$*  and the lack of *dpr2*,

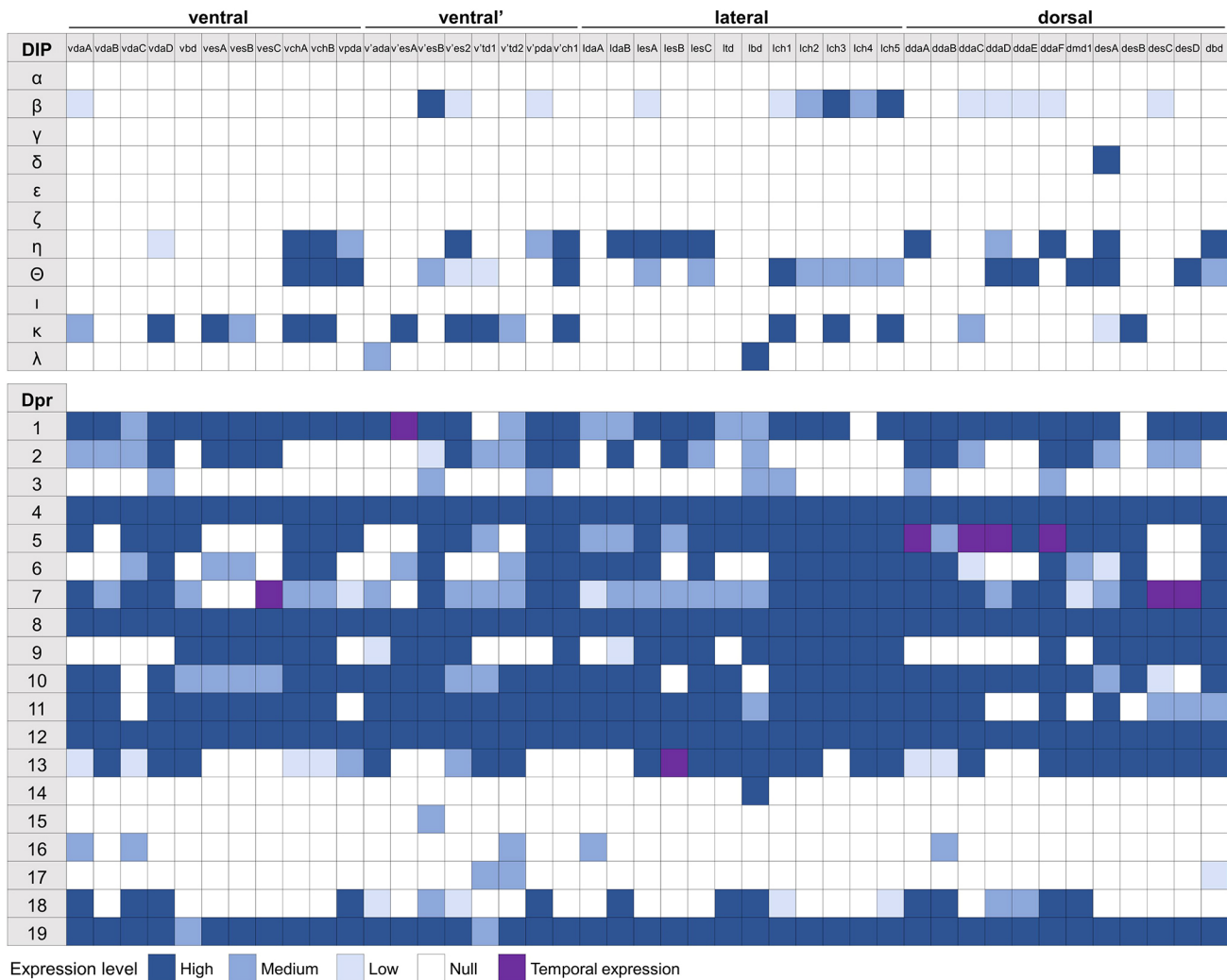


**Fig. 5. Expression map of Dpr and DIP genes in all larval SNs.** Each column represents an SN. Expression of each gene in each SN is characterized into a specific category as indicated in the key.

*dpr6*, *dpr9*, *dpr11* and *dpr13*, and da-II/da-III neurons are grouped by expression of *dpr2* and *dpr18*, and the lack of *dpr9* (Fig. 6A). These results suggest that SNs in the same type/class may utilize similar sets of Dpr and DIP genes to recognize common interneuron targets.

#### Expression of Dpr and DIP genes is more diversified in MNs

Next, we examined whether MNs that project to the same muscle groups also share the same expression patterns of Dpr and DIP genes. Muscles are grouped into three main spatial and functional groups – ventral, lateral, dorsal – and further divided into six subgroups based on their orientation – dorsal longitudinal (DL), dorsal oblique (DO), ventral longitudinal (VL), ventral oblique (VO), ventral acute (VA) and lateral transverse (LT) (Fig. 1B) (Bate, 1990; Hooper, 1986; Zarin et al., 2019). Each muscle is normally innervated by one Ib MN and previous studies showed that Ib MNs innervating a muscle group project their dendrites to the same region in the VNC neuropil where they receive input from common premotor neurons (Kim et al., 2009; Landgraf and Thor, 2006; Landgraf et al., 1997, 2003b; Mauss et al., 2009; Zarin et al., 2019). Thus, if Ib MNs of the same muscle group share premotor neuron partners, they may share wiring molecules. We generated an unbiased hierarchical clustering based on expression of Dpr and DIP

genes for all MNs (Fig. 6B). Type-Is, type-II and type-III MNs form independent clusters and are distinct from Ib MNs. For example, *DIP-α*, *DIP-ζ*, *dpr6* and *dpr16* are expressed in type-Is MNs, and lateral and dorsal type-II MNs are identified by the lack of *DIP-κ*, *dpr15* and *dpr17* and the expression of *dpr3* and *dpr16* (Fig. 6B). However, within Ib MNs, only the MNs innervating LT and DL muscles are clustered together, whereas the other MNs appear randomly distributed. These results suggest that, based on the expression patterns of Dpr and DIP genes, MNs can be clustered by their type, but Ib MNs cannot be further clustered by the muscles they innervate. MNs must identify distinct pre- and postsynaptic partners, which may explain the inability to cluster Ib MNs based on their expression patterns of Dpr and DIP genes. Therefore, more complex identification codes may be necessary for MNs to distinguish both pre- and postsynaptic partners.

#### Dpr and DIP gene expression maps reveal additional MNs Alary muscle MN

In addition to the muscles required for larval locomotion, larvae have another segmentally repeated muscle, the alary muscle, which attaches to the trachea along the larval heart tube (Bataillé et al., 2015). The alary muscle MN axon resides in the transverse nerve (TN) and projects along m8 towards the alary muscle. Here, we



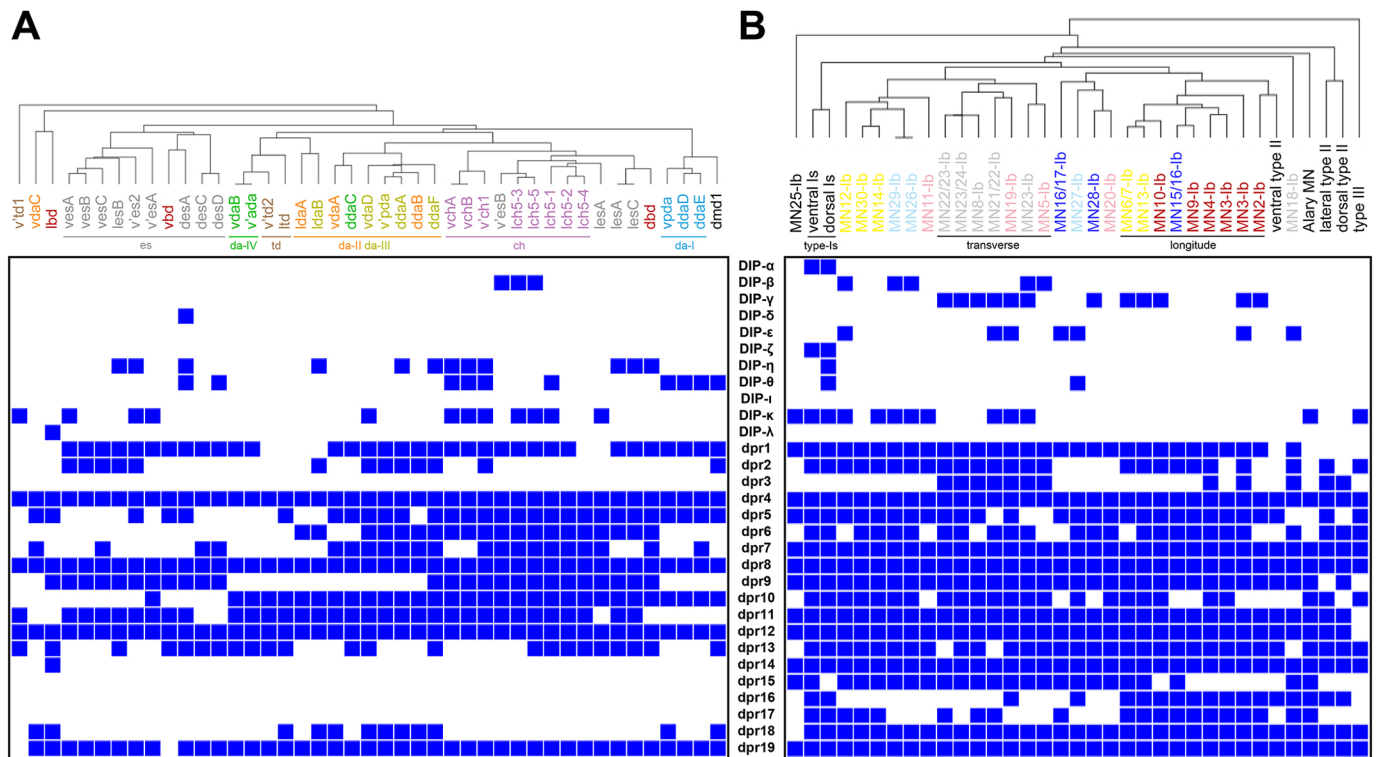


**Fig. 6. Hierarchical clustering of SNs and MNs reveals shared expression patterns of Dpr and DIP genes in neurons from the same class.** (A) SNs from the same class are clustered together based on their expression pattern of Dpr and DIP genes. For example, most es neurons (gray), all chordotonal neurons (purple), and da neurons fall into distinct clusters. (B) Modulatory MNs (II and III) and type-Is MNs are distinct from the main type-Ib cluster. However, individual type-Ib MNs are not easily distinguished based on their expression of Dpr and DIP genes.

mapped the expression of Dpr and DIP genes in the alary muscle MN. As previously observed, the dendrite of the lbd neuron travels in parallel with the alary muscle MN axon within the TN (Gorczyca et al., 1994; Macleod et al., 2003; Thor and Thomas, 1997). Thus, if a Dpr or DIP gene is expressed in both the alary muscle MN and lbd, we would be unable to distinguish them in the nerve. Therefore, we monitored the colocalization of DLG and the fluorescent reporter on the alary muscle to assign expression unambiguously (Fig. S9). We observed that alary muscle MN NMJs share features of type-I boutons, including the size and DLG labeling surrounding the boutons. Using the same criteria described for MNs and SNs, we found one DIP gene and many Dpr genes that are expressed in the alary muscle MN, including *DIP-κ*, *dpr4* and *dprs7-19*. These expression data and driver lines will facilitate future characterization of this MN.

### MN23-Ib

Most Ib MNs have a single muscle target. However, some Ib MNs innervate two muscles in close proximity, likely due to shared recognition cues. For example, a previous study found that Ib MNs innervating the lateral muscles can synapse with neighboring muscles and thus named these neurons MN21/22-Ib, MN22/23-Ib and MN23/24-Ib (Fig. 7A) (Hoang and Chiba, 2001). These innervation patterns were later confirmed by MARCM (mosaic analysis with a repressible cell marker) analysis (Kim et al., 2009).

In our analyses, we observed that m23 has several Ib NMJ branches and m24 has only one NMJ (Fig. 7B). Although a single MN can form several branches on a muscle, we found some *dpr/DIP-GAL4* lines that only label one Ib branch on m23 and no other branches on lateral muscles (Fig. 7C). These data suggest the

existence of an additional MN that solely innervates m23, and we named it MN23-Ib. The bouton size and DLG labeling intensity of MN23-Ib boutons indicates that it is a type-Ib NMJ. *DIP-β* and *DIP-κ* are expressed in MN23-Ib and not in the nearby MN22/23-Ib and MN23/24-Ib (Fig. 7C). Note that MN23/24-Ib forms long, linear Ib NMJs on the underside of m23 before it reaches m24 (Fig. 7A,C). We also found that *dpr5* was expressed in MN23/24-Ib and nearby MN22/23-Ib, but not in MN23-Ib (Fig. 7D), providing further evidence for an additional Ib MN solely innervating m23. Additional Dpr and DIP genes are expressed in both MN23-Ib and MN23/24-Ib (Fig. 7B). Thus, we describe a previously unidentified Ib MN that innervates m23.

### MN6-Ib and MN7-Ib in A2

Another example of a dual-targeting Ib MN is MN6/7-Ib (also known as RP3 in the embryo) (Schmid et al., 1999; Sink and Whittington, 1991a,b). The innervation pattern of MN6/7-Ib was initially identified by dye-fill labeling and MARCM (Hoang and Chiba, 2001; Kim et al., 2009; Sink and Whittington, 1991b). Owing to the ease of accessibility of m6 and m7, MN6/7-Ib is extensively used for studies of synaptic connectivity, synaptic growth and synaptic homeostasis.

Based on these previous studies, we predicted that if a Dpr or DIP gene were expressed in MN6/7-Ib, the Ib NMJs on both m6 and m7 would be completely fluorescently labeled (Fig. 8A, right). Surprisingly, in A2, we observed several *dpr/DIP-GAL4*s that label Ib MNs that have large NMJs on m6 and others that label mainly the Ib NMJs on m7 (Fig. 8A, left). For example, *DIP-β*, *DIP-γ* and *DIP-ε* were expressed in an MN that mainly innervates m6 (Fig. 8B), whereas *dpr15* was expressed in an MN that mainly

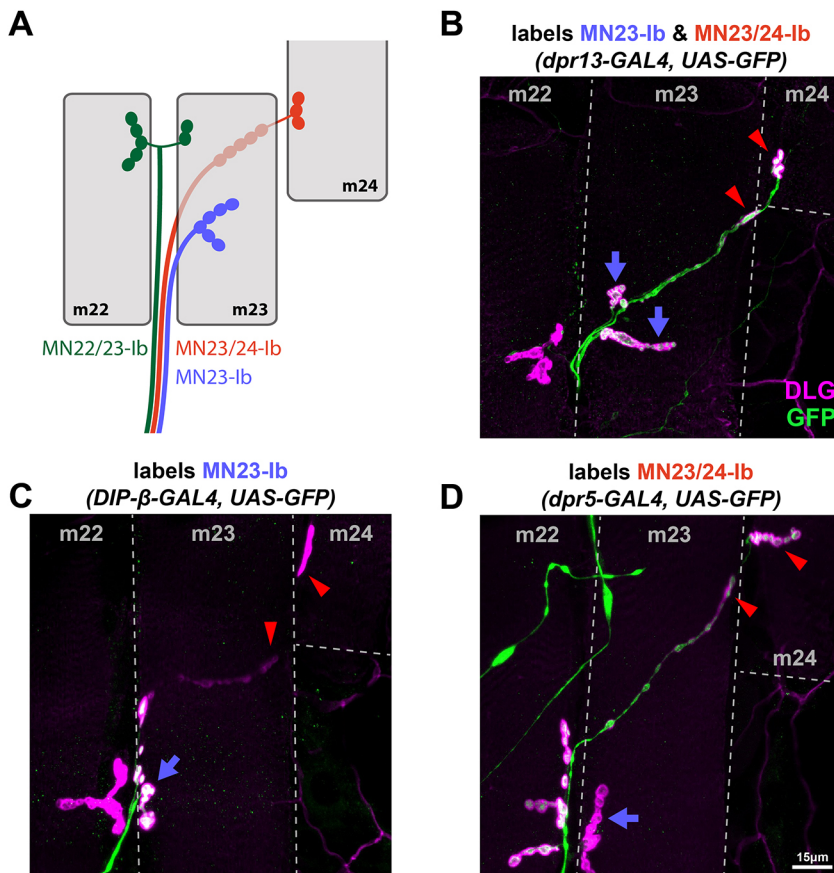


**Fig. 7. Differentially expressed Dpr and DIP genes reveal an MN that solely innervates m23.** (A) Schematic of transverse muscles 22, 23 and 24 (gray) with previously identified MN22/23-Ib (green), MN23/24-Ib (red) and newly identified MN23-Ib (blue). (B) Representative image showing *dpr13-GAL4* expression in both MN23/24-Ib (red arrowheads) and MN23-Ib (blue arrows). Thus, all boutons on m23 and m24 are labeled by GFP. (C) Representative image showing *DIP-β-GAL4* expression in MN23-Ib (blue arrow). Boutons underneath m23 and boutons from m22, m24 (red arrowheads) are not labeled by GFP, thus *DIP-β-GAL4* is not expressed in MN22/23-Ib and MN23/24-Ib. (D) Representative image showing *dpr5-GAL4* expression in MN22/23-Ib and MN23/24-Ib (red arrowheads), but not in MN23-Ib (blue arrow). The lack of GFP in the arbor on m23 indicated the existence of an MN that solely innervates m23.

innervates m7 (Fig. 8C). These expression patterns suggested that two Ib MNs innervate m6 and m7 in A2. Hereafter, we named these MNs as MN6-Ib and MN7-Ib. Prior studies hinted at the possibility of two MNs based on the larger synaptic terminal area on m6/7 in A2 compared with A3–A6 (Lnenicka and Keshishian, 2000). However, it was thought that the larger synaptic area was due to a large NMJ from a single Ib MN. In the larval neuromuscular circuit, the number of boutons reflects the size of the NMJ. We quantified the m6 and m7 Ib NMJs and observed a significantly larger arbor in A2 compared with A3 (Ib NMJ on m6: 34.2 on A2 and 18.5 on A3; Ib on m7: 23.1 on A2 and 11.7 on A3) (Fig. S10). Taken together, we conclude that m6 and m7 in A2 are innervated by two Ib MNs.

#### Characterization of MN6-Ib and MN7-Ib

A recent study reported a GAL4 driver (*GMR79H07-GAL4*) that labels MN6-Ib in A2 (Aponte-Santiago et al., 2020). We tested this driver and confirmed MN6-Ib expression; however, it sometimes labels MN7-Ib NMJs or both MN6-Ib and MN7-Ib (Fig. S11). We examined MN6-Ib and MN7-Ib further in order to understand better their innervation patterns and dendritic projections. Interestingly, we found that MN6-Ib and MN7-Ib preferentially innervate their corresponding muscle, but sometimes these MNs also form minor NMJs on the neighboring muscle (Fig. 8A). Next, we monitored the frequency of dual innervation of each MN using *GMR79H07-GAL4* and found that 68.2% of MN6-Ib and 72.7% of MN7-Ib innervate both muscles (Fig. 9A). We also determined the size of each NMJ by counting Ib boutons and found that on average MN6-Ib forms 48.6 boutons on m6 and 5.9 boutons on m7, whereas MN7-Ib forms 3.1 and 30.8 boutons on m6 and m7, respectively (Fig. 9B).

MN6/7-Ib (RP3) is derived from neuroblast 3-1 (NB3-1) (Schmid et al., 1999; Sink and Whittington, 1991a,b). To visualize the

dendritic projections of MN6-Ib and MN7-Ib in A2, we examined their cell body position in the VNC and dendrite morphology using a pan-MN driver, *OK6-GAL4*, with multi-color FLP-out (MCFO) (Nern et al., 2015). We found that the cell bodies of MN6-Ib and MN7-Ib are both localized at the dorsal neuropil and project axons to the contralateral hemineuromere. They also extend a small dendritic arbor to the ipsilateral side (Fig. 9C–F). These features are shared with RP3 (MN6/7-Ib) (Kim et al., 2009). These data suggest that these two MNs likely both originated from NB3-1. Overall, we identified and confirmed the presence of two Ib MNs in A2 that preferentially innervate m6 or m7.

#### DISCUSSION

Dprs and DIPs play important roles in nervous system development, and they are widely expressed across many neural circuits. Several groups have utilized the GAL4/UAS system to visualize expression of Dpr and DIP genes in olfactory neurons (Barish et al., 2018), adult leg MNs and SNs (Venkatasubramanian et al., 2019), optic lobe neurons (Cosmanescu et al., 2018; Tan et al., 2015) and fru P1 neurons (Brovero et al., 2021). Although these studies revealed unique Dpr and DIP gene expression in the respective neurons, the depth of the expression maps was limited due to the less complete GAL4 collection at the time, and some studies only focused on a global expression pattern without characterization of individual cell types.

Here, we reported a collection of GAL4 enhancer trap lines for all DIP genes and 19 Dpr genes, and examined their expression in larval MNs, muscles, peripheral glia and SNs. Interestingly, we found that many Dpr and DIP genes are expressed in patterns including different expression levels, anterior-posterior gradients and temporal expression. Our expression analyses also revealed previously uncharacterized larval MNs that differentially express

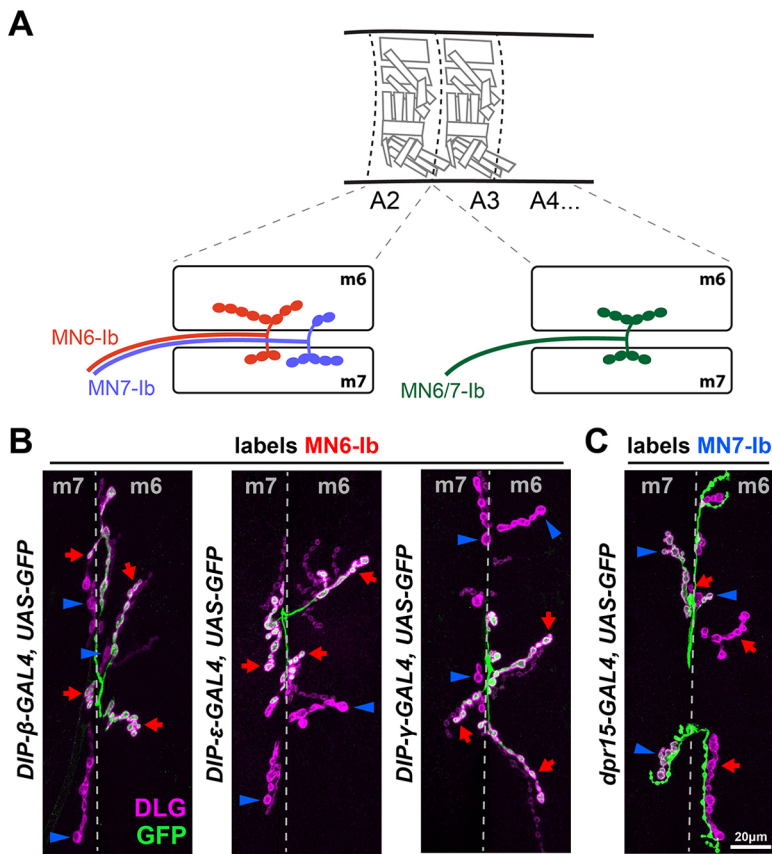


**Fig. 8. Differentially expressed Dpr and DIP genes reveal MN6-Ib and MN7-Ib in segment A2.** (A) Schematic of MN6-Ib (red) and MN7-Ib (blue) in segment A2, and MN6/7-Ib (green) in A3-A7. MN6-Ib preferentially innervates m6 but also forms a small NMJ on m7, whereas MN7-Ib prefers m7 but also forms a small NMJ on m6. (B) Representative images showing that *DIP-β*, *DIP-ε* and *DIP-γ* are specifically expressed in MN6-Ib (red arrows), but not in MN7-Ib (blue arrowheads). Note that MN6-Ib forms boutons with both m6 and m7, as there is a small GFP-positive type-Ib NMJ on m7 (red arrows on m7). Conversely, the lack of GFP in most m7 type-Ib NMJ and the small m6 type-Ib NMJ (blue arrowheads) also indicate dual innervation of both muscles by MN7-Ib. (C) Representative image showing that *dpr15* is specifically expressed in MN7-Ib (blue arrowheads) but not in MN6-Ib (red arrows). MN6-Ib and MN7-Ib also show dual innervation patterns in this genetic background.

Dpr and DIP genes. The Dpr and DIP gene expression maps identified here, along with the GAL4 lines that are also hypomorphs or loss-of-function alleles, will facilitate examination of Dpr-DIP interactions in development of motor, sensory, and many other circuits.

### Insights from Dpr and DIP gene expression maps to aid functional studies

The goal of developing expression maps for Dpr and DIP genes in MNs and SNs is to instruct the functional study of Dpr-DIP interactions. Here, we discuss testable hypotheses based on our expression maps that may serve as an entry point for future research.

Based on our expression map, all muscles express *dpr19* and most also express *dpr10*. Dpr10 and Dpr19 interact with *DIP-α/β/λ* and *DIP-ε/ζ*, respectively, and a majority of MNs express at least one of these DIPs. Thus, Dpr-DIP interactions could instruct MN-muscle recognition and/or act combinatorially with other synaptic connectivity molecules. However, some MNs do not express any of these DIPs, suggesting that other pairs of CSPs are involved in MN-muscle recognition. Alternatively, muscles may express unknown Dpr or DIP interactors not tested in the previous biochemical screen. In addition, we found many Dpr-DIP interactors that were co-expressed in the same MNs. For example, *DIP-β* and its interacting partners, *dpr6/8/9/11*, are co-expressed in MN12-Ib, suggesting that Dpr-DIP *cis* interactions may contribute to NMJ development and connectivity.

Another way to approach the function of Dpr-DIP interaction is focusing on the commonly or differentially expressed Dpr and DIP genes. Hierarchical clustering analyses of SNs grouped SNs from the same class together based on the expression of Dpr and DIP genes, suggesting that similar SNs have common Dpr and DIP genes.

Future studies could determine the Dpr and DIP gene expression maps in the downstream interneurons to identify synaptic partners that express cognate Dpr-DIP pairs. However, one should also note that cluster analysis based solely on binary Dpr and DIP gene expression ignores expression levels and localization of proteins, which are important determinants for circuit wiring. Combining these with other parameters, such as transcription factor expression, can refine the clustering results and reduce unlikely correlations.

Instead of commonly expressed genes, differentially expressed Dpr and DIP genes in similar projecting neurons could shed light on connectivity mechanisms. For example, MN6-Ib and MN7-Ib, identified in this study, have similar morphology and innervation patterns, but with a preference for m6 and m7, respectively. One interesting question is how these neurons distinguish their muscle targets to generate such preference. Based on the expression map, MN6-Ib and MN7-Ib co-express a large subset of Dpr and DIP genes, but *DIP-β*, *DIP-γ*, *DIP-ε* and *dpr15* are selectively expressed. These differentially expressed genes are excellent candidates to explore the recognition mechanism of these MNs. Similar approaches could be adapted to other MNs that innervate neighboring muscles.

The Dpr-DIP interactome (Carrillo et al., 2015; Cosmanescu et al., 2018; Özkan et al., 2013) revealed binding promiscuity in the interactions and our expression maps showed that many cells co-express many Dpr and DIP genes, suggesting redundant mechanisms for synaptic recognition. Several subfamilies of CSPs are implicated in recognition, but loss-of-function mutants rarely are 100% penetrant. For example, loss of Teneurin signaling causes a 90% decrease of MN3-Ib innervation (Hong et al., 2012), and Toll null mutants revealed defects in 35% of MN6/7-Ib (Rose et al., 1997). These data suggested that other CSPs are required in the



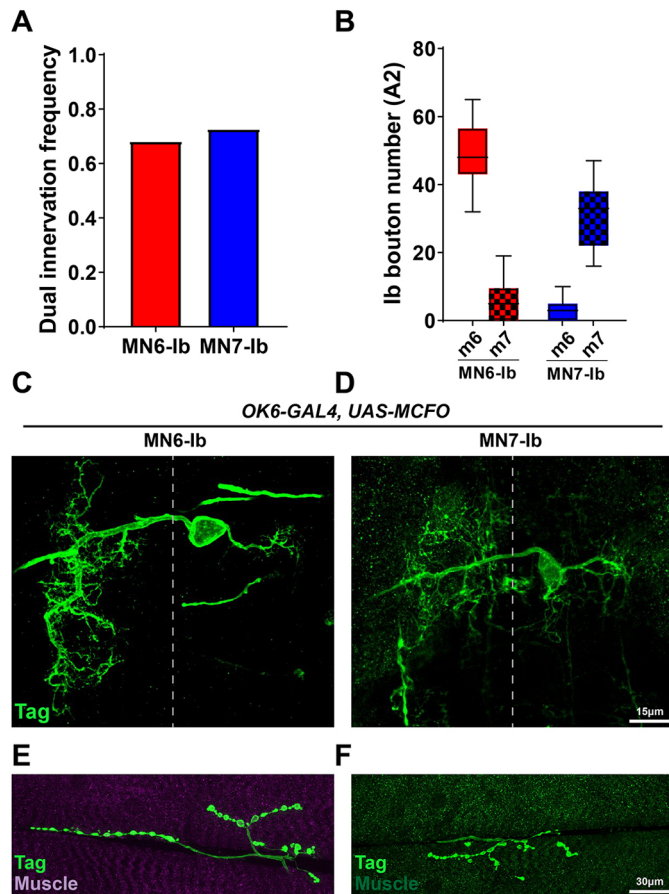


**Fig. 9. Further characterization of MN6-Ib and MN7-Ib.** (A) Quantification of the dual innervation frequencies of MN6-Ib and MN7-Ib: 68.2% of MN6-Ib also innervate m7 and 72.7% of MN7-Ib also innervate m6 ( $n=21$  hemisegments). (B) Quantification of MN6-Ib and MN7-Ib NMJ sizes on both muscles ( $n=21$  hemisegments). (C, D) A pan-MN driver *OK6-GAL4* driving *MCFO* revealed the dendritic morphology of MN6-Ib and MN7-Ib in the VNC. (E, F) Corresponding NMJ images from the same neuron shown in C (MN6-Ib) and D (MN7-Ib).

recognition between MNs and their respective muscles. Utilizing the Dpr and DIP gene expression maps, co-expressed Dpr and DIP genes could be simultaneously knocked out in specific MN or SN to examine redundancy. For example, the dorsal Is MN expresses six DIPs, and *DIP- $\alpha$*  is required for Is innervation of m4 but only partially required for Is innervation of other muscles. If redundant DIP codes are required for specific innervations, a sextuple DIP mutant should reveal complete loss of dorsal Is NMJs.

### CSP expression patterns in the fly nervous system

CSPs can serve several functions in nervous system development, including molecular codes for partner recognition and self-avoidance. CSP expression patterns can suggest different functions; the expression of CSPs could be deterministic to instruct stereotyped synaptic connectivity or stochastic to avoid dendritic overlap and self-synapses. For example, *Capricious* is robustly expressed in MN12-Ib and some dorsal MNs (Nose, 2012; Shishido et al., 1998), and loss-of-function and gain-of-function approaches have revealed neuromuscular wiring defects, suggesting that the robust expression of *Capricious* instructs synaptic partner recognition. In our study, we showed that many Dpr and DIP genes are robustly expressed in SNs and MNs, indicating their potential roles in synaptic wiring.

By contrast, some CSPs are stochastically expressed in subsets of cells. For example, probabilistic splicing of *Dscam1* generates random isoform expression in SNs to mediate dendritic self-avoidance by inhibitory homophilic interactions (Miura et al., 2013). Interestingly, we found that many Dpr and DIP genes are also stochastically expressed in MNs and SNs. Such irregular expression patterns may suggest additional functions of Dpr and DIP genes in circuit formation.

In this study, we also uncovered some Dpr and DIP genes that are expressed in a gradient along the anterior-to-posterior axis. Such patterns are reminiscent of the expression of several Hox genes in the VNC. For example, *Ubx* and *Abd-A* are highly expressed in anterior segments whereas *Abd-B* is mainly in the posterior (Estacio-Gómez and Díaz-Benjumea, 2013; Meng and Heckscher, 2020). These transcriptional factors were proposed to set up segmental cues in the nervous system, but the downstream genes and pathways are not completely understood. The similar expression patterns suggest that gradient transcriptional factors may regulate segmental development, in part, through Dpr and DIP genes.

### *dpr/DIP-GAL4* collection to enable neuron identification and manipulation

The maps of *Drosophila* MNs and SNs was established decades ago using dye backfills (Broadus et al., 1995; Hoang and Chiba, 2001; Landgraf et al., 2003a). However, fluorescent dyes have some technical limitations as they do not always flow into every terminal structure, which may have resulted in some neurons being overlooked. In this study, we used a genetic approach to probe individual neurons and revealed three uncharacterized MNs: MN23-Ib, MN6-Ib (A2) and MN7-Ib (A2).

In addition, the *GAL4* lines in this study provide genetic access to manipulate subsets of neurons. In the *Drosophila* motor circuit, several studies have identified reporters that are expressed in subsets of motor neurons, muscles and interneurons (Aponte-Santiago et al., 2020; Li et al., 2014; Pérez-Moreno and O’Kane, 2018; Wang et al., 2021). However, the coverage of these reporters is very limited (i.e. only a small number of cells can be targeted). To generate new genetic tools for targeting subsets of MNs, the Dpr and DIP gene expression maps could be inspected for partially overlapping or non-overlapping *dpr/DIP-GAL4* expression and converted to split-*GAL4* or *GAL80*, respectively. Thus, the expression data in the present study and the MiMIC/CRIMIC lines provide a pipeline to expand the genetic toolbox and to label and manipulate neurons in a highly specific manner.

### Using the Dpr/DIP gene code to annotate single-cell RNA sequencing data

Recent advances in single-cell RNA sequencing (scRNAseq) provide a powerful, high-throughput approach to identify large-scale gene expression patterns. Various *Drosophila* neural tissues have been analyzed by scRNAseq (Li, 2020). However, most studies report the transcriptome of large cell clusters, including MNs, ganglion cells, neuroblasts and glial cells because of the difficulty of matching single-cell reads to a specific cell type and identity, impeding detailed analyses from scRNAseq data.

One method to deconvolve these large cell clusters is sorting cells before performing scRNAseq. Researchers may also use the scRNAseq data to identify specific drivers, and then identify which neuron expresses this driver (Simon and Konstantinides, 2021). However, this approach reduces the scale because only a few cell types can be identified in this manner. Utilizing the expression of a gene family known to be differentially expressed within a

specific subset of cells can provide a more complete examination. For example, the Dpr and DIP gene expression maps would generate a cell-specific atlas to annotate clusters in scRNAseq data and help to identify individual MNs from an MN cluster in a larval VNC sample (Nguyen et al., 2021; Vicidomini et al., 2021). In addition to Dpr and DIP genes, other CSP subfamilies have been reported in several scRNAseq datasets, suggesting that expression maps of other subfamilies and even combinations of subfamilies can be utilized to refine cell types in datasets (Kurmangaliyev et al., 2020; Ma et al., 2021; Xie et al., 2021).

### Limitations of using GAL4 lines to profile expression patterns

In the current study, we present expression maps of Dpr and DIP genes in a variety of cells using a GAL4 collection. However, several caveats exist. First, using a GAL4/UAS approach will not provide spatial information about where Dprs and DIPs are localized subcellularly, e.g. in axons or dendrites. Future work will generate endogenously tagged versions of, or antibodies against, Dprs and DIPs. In addition, using the current GAL4/UAS pipeline, we cannot unequivocally identify specific interneurons that express Dpr and DIP genes because of their indistinguishable cell morphologies in the densely packed VNC. Transcription factor staining and generation of split GAL4s can reveal interneurons identities but at relatively low throughput. Finally, utilizing a lineage-tracing system, we uncovered temporally expressed Dpr and DIP genes. However, neither of our approaches revealed when Dpr and DIP genes were first expressed. Embryo or early-stage larval dissection will provide more temporal resolution.

## MATERIALS AND METHODS

### Drosophila lines

All *dpr/DIP-GAL4* lines are listed in Table S1. Other driver lines were: *OK6-GAL4* (Bloomington *Drosophila* Stock Center, 64199), *GMR79H07-GAL4* (gift from Troy Littleton, MIT, MA, USA), *MHC-GAL80* (gift from Timothy Mosca, Thomas Jefferson University, PA, USA). Reporter lines were: *10XUAS-mCD8::GFP* (Bloomington *Drosophila* Stock Center, 32184), *20XUAS-mCherry* (Bloomington *Drosophila* Stock Center, 52268), *UAS-2XEGFP*; *actin-(FRT.STOP)-GAL4, UAS-FLP* (permanent reporter, gift from Ellie Heckscher, University of Chicago, IL, USA), *UAS-RedStinger, UAS-FLP, Ubi-p63E(FRT.STOP)-Stinger* (G-TRACE; Bloomington *Drosophila* Stock Center, 28280), *R57C10-FLP::UAS-MCFO* (Bloomington *Drosophila* Stock Center, 64089). Lines used to generate Trojan-GAL4 were: *yw; Sp/CyO; loxP(Trojan-GAL4)x3* (Bloomington *Drosophila* Stock Center, 60311), *yw; loxP(Trojan-GAL4)x3; Dr/TM3, Sb, Ser* (Bloomington *Drosophila* Stock Center, 60310), *yw, hs-Cre, vas-phiC31::int* (Bloomington *Drosophila* Stock Center, 60299).

### Antibodies

Primary antibodies used in this study were: rabbit anti-GFP (1:40,000; gift from Michael Glozter, University of Chicago, IL, USA), rabbit anti-HA (1:1000; Cell Signaling Technology, C29F4), mouse anti-DLG (1:100; Developmental Studies Hybridoma Bank, 4F3), mouse anti-Repo (1:100; Developmental Studies Hybridoma Bank, 8D12), mouse anti-Myosin (1:100; Invitrogen, A31466), chicken anti-GFP (1:500; Invitrogen, A10262), chicken anti-RFP (1:500; Novus Biologicals, NBP2-25158), chicken anti-V5 (1:500; Bethyl Laboratories, A190-118A), rat anti-Flag (1:200; Novus Biologicals, NBP1-06712).

Secondary antibodies used were: goat anti-rabbit Alexa 488 (1:500; Invitrogen, A11008), goat anti-rabbit Alexa 568 (1:500; Invitrogen, A11036), goat anti-mouse Alexa 568 (1:500; Invitrogen, A11031), goat anti-mouse Alexa 647 (1:500; Invitrogen, A32728), goat anti-chicken Alexa 488 (1:500; Invitrogen, A11039), donkey anti-chicken Cy3 (1:500; Jackson ImmunoResearch, 703-165-155), goat anti-rat Alexa 647 (1:500; Invitrogen, A21247), goat anti-HRP Alexa 647 (1:100; Jackson

ImmunoResearch, 123-605-021), goat anti-Phalloidin Alexa 405 (1:100; Invitrogen, A30104).

### Fly genetics

When examining available *dpr/DIP-GAL4* lines to confirm the GAL4 insertion sites and the version of GAL4 used, we found that the original *dpr13-GAL4* no longer contained the GAL4 sequence (Barish et al., 2018; Brovero et al., 2021). Therefore, we generated new *dpr13-GAL4* and *dpr8-GAL4* from respective MiMIC insertion lines using Trojan exons (Diao et al., 2015). To generate *DIP-λ* CRIMIC insertions, gRNA (5'-AGCATCTATCGCTTGTGAAAGGG-3') was designed to target the coding intron. The insertion sites and GAL4 versions are indicated in Table S1.

### qRT-PCR

Five larvae per genotype were collected and homogenized using pellet pestles (Fisher Scientific). All samples tested contained a mix of males and females, except for *dpr8-GAL4*, for which only females were used due to its location on the X chromosome and homozygous lethality. RNA was extracted using RNAqueous Total RNA Isolation Kit (Thermo Fisher, AM1912) and subsequently treated with DNaseI for 30 min at 37°C to remove genomic DNA. cDNA was generated from 1 µg of RNA using random hexamers and SuperScript IV First-Strand Synthesis System (Thermo Fisher, 18091050) and RNA was removed using RNase H at 37°C for 20 min. Primers were designed to be 18-23 bp long, amplify 100-200 bp, and have a melting temperature of ~60°C (Table S2). All primer locations are downstream of mapped GAL4 insertion sites and were validated with control cDNA. qRT-PCR was performed with Power SYBR Green PCR Master Mix (Bio-Rad, 4368577) and run on a QuantStudio 3 real-time PCR system (Thermo Fisher). All reactions were normalized to the housekeeping gene *RpL32* and control flies, yielding  $\Delta\Delta Ct$  values (Ponton et al., 2011). Relative fold change was calculated as  $2^{-\Delta\Delta Ct}$ . Each reaction was run in technical and biological triplicate.

### Dissection and immunocytochemistry

Larval dissections and immunostaining were performed as previously described (Ashley et al., 2019). Briefly, wandering third instar larvae were dissected along the dorsal midline in PBS on a Sylgard plate and stretched out with insect pins. To visualize alary muscles, larva was dissected from the ventral side. Dissected body walls were washed once with PBS and fixed for 30 min with 4% paraformaldehyde. Samples were then washed three times with PBT (PBS+0.05% Triton X-100). Samples were incubated with primary antibody at 4°C overnight, washed three times with PBT, and then incubated in secondary antibody at room temperature for 2 h. Samples were finally mounted in 30 µl vectashield (Vector Laboratories). Representative images were taken with a Zeiss LSM800 confocal microscope with a 40× Plan-Neofluar 1.3 NA objective and processed with ImageJ.

### Examining expression of Dpr and DIP genes in MNs and SNs

We dissected six third instar larvae from each cross and immunostained for GFP/RFP, DLG and HRP. Mounted samples were examined under a Zeiss AxioImager M2 with a Lumen light engine with a 20× Plan Apo 0.8 NA objective. Each sample was examined twice with the same criteria to reduce human error. To map the expression of Dpr and DIP genes in MNs, NMJs were identified by labeling for DLG or HRP, and then examined for GFP/RFP colocalization. For expression in SNs, SN cell bodies were located by HRP labeling, and then examined for GFP/RFP colocalization. We counted all MNs and SNs from anterior to posterior hemisegments (abdominal segments A2-A7) to gain a full Dpr and DIP gene expression map across the body wall. Note that we did not observe the third type-Is MN (MNSNa-Is) described by Hoang and Chiba (2001). The pipeline and criteria of determining the expression level is described below (Fig. S4).

In *dpr/DIP-GAL4>GFP/RFP* animals, if the reporter gene was expressed constantly in a specific MN/SN in all hemisegments, then this GAL4 line was counted as 'high expression level' in this MN/SN. If the fluorescent reporter was not expressed consistently in a specific MN/SN, then: (1) if the fluorescent reporter showed a gradient increase or decrease along the



anterior to posterior axis, then the expression of this GAL4 line was reported as ‘gradient increase’ or ‘gradient decrease’, respectively; or (2) if the reporter gene was not expressed in a gradient, but was randomly expressed in a specific MN/SN, then the expression was counted as ‘medium expression level’ in this MN/SN. Note that we did not record gradient expression for SNs, because the reporter expression was more variable in SNs compared with MNs.

In the cross between *dpr/DIP-GAL4* and the permanent labeling reporter, we first confirmed the high, medium and gradient expression level described above. Then, if a GAL4 line showed no expression in the cross to *UAS-GFP/RFP* but did show expression in the cross to the permanent labeling reporter, we counted how frequently this MN/SN was labeled: (1) if the labeling frequency was lower than 30% across all hemisegments, then this GAL4 was recorded as ‘low expression level’ in this MN/SN because the expression could be too low to detect in the cross to *UAS-GFP/RFP* but sufficient to trigger some FLP-out; (2) if the labeling frequency was between 30% and 60%, then this GAL4 expression was recorded as ‘medium expression level’ in this MN/SN; (3) if the labeling frequency was higher than 60%, then this GAL4 expression was considered as ‘temporal expression’ as it indicates a high GAL4 expression level temporally in early developmental stages because it triggers high frequency FLP-out. Finally, if a GAL4 was not expressed in both the cross to *UAS-GFP/RFP* or permanent reporter, it was recorded as ‘null expression’.

*dpr10-GAL4* was crossed to *UAS-GFP* together with *MHC-GAL80* to prevent muscle GFP expression, because a high level of muscle GFP would mask NMJs and SN cell bodies. In addition, *Dpr* genes with muscle expression (*dpr10* and *dpr19*) were not crossed to the permanent labeling reporter.

### Examining expression of Dpr and DIP genes in glia and muscles

We examined expression of *Dpr* and *DIP* genes in glia and muscles with the G-TRACE reporter (Evans et al., 2009). We dissected six larvae from each cross and immunostained for GFP, RFP, HRP and Repo. Glial expression was confirmed by GFP/RFP colocalization with Repo. Muscle expression was confirmed by GFP/RFP-positive muscle nuclei. Although the cross to *UAS-GFP/RFP* and the permanent labeling line also showed muscle expression, the diffusible GFP signal impeded the clear distinction of muscle boundaries.

### Hierarchical clustering using Dpr and DIP gene expression

To perform hierarchical clustering, the expression of *Dpr* and *DIP* genes were first converted to binary values of ‘0’ and ‘1’. Robust expression, including high expression and temporal expression, were considered as ‘1’, whereas medium and low expression, and gradient expression were considered as ‘0’. We reasoned that robust expression of *Dpr* and *DIP* genes may suggest more a significant role in the respective cell. Binary data were subjected to hierarchical analysis using Morpheus (Broad Institute) (Metric: Cosine Similarity; Method: Average). Figures were exported and color coded in Adobe Illustrator to indicate different types of MNs and SNs.

### Bouton number and dual innervation counting

To quantify m6 and m7 NMJs in wild-type animals, we located Ib NMJs by DLG labeling and counted bouton number by HRP labeling. To measure the MN6-Ib or MN7-Ib NMJ sizes in *GMR79H07-GAL4>GFP* animals, we first looked for GFP colocalization with DLG to distinguish MN6-Ib and MN7-Ib. For example, if the major Ib arbor on m6 is GFP positive, then it is formed by MN6-Ib, and the GFP-negative boutons are formed by MN7-Ib. We then counted the bouton numbers of each Ib arbor by HRP labeling. Unpaired, two-tailed Student’s *t*-test was used for comparison between two groups (followed by Welch’s correction in cases of unequal variance, Prism 8). Error bars indicate s.e.m.

### Acknowledgements

We thank the *Drosophila* Gene Disruption Project for generating MiMIC and CRIMIC insertion lines. Stocks obtained from the Bloomington *Drosophila* Stock Center (NIH P40OD018537) were used in this study. The hybridomas 4F3 and 8D12 were developed by Corey Goodman, and obtained from the Developmental Studies Hybridoma Bank, created by the NICHD of the NIH and maintained at The University

of Iowa, Department of Biology, Iowa City, IA 52242. We thank Troy Littleton (MIT), Lawrence Zipursky (UCLA) and Michelle Arbeitman (FSU) for sharing fly lines. We also thank Kai Zinn, Edwin ‘Chip’ Ferguson, Richard Fehon, Ellie Heckscher, David Pincus, Martha Plutarco Jr and members from the Carrillo laboratory for valuable discussions and comments. Some figure components were created with BioRender.com.

### Competing interests

The authors declare no competing or financial interests.

### Author contributions

Conceptualization: Y.W., J.A., R.A.C.; Formal analysis: Y.W., M.L.-R.; Investigation: Y.W., M.L.-R., J.A., V.A., P.C.; Resources: Y.W., J.A., H.J.B., O.K.; Writing - original draft preparation: Y.W., R.A.C.; Writing - review and editing: Y.W., M.L.-R., J.A., H.J.B., O.K., R.A.C.; Supervision: R.A.C.; Funding acquisition: M.L.-R., H.J.B., R.A.C.

### Funding

This work was supported by the National Institute of Neurological Disorders and Stroke (R01 NS123439 01), the National Science Foundation (IOS-2048080), and a University of Chicago Faculty Diversity Grant and Pilot Project Grant to R.A.C. and the National Institute of General Medical Sciences (T32 GM007183) and National Institute of Neurological Disorders and Stroke (F31NS120458) to M.L.-R. This work is also supported by funds from the University of Chicago Biological Science Division, Committee of Developmental Biology and Department of Molecular Genetics and Cellular Biology. Further support came from the Office of Research Infrastructure Programs, National Institutes of Health (awards R24 OD022005 and R24 OD031447 to H.J.B.). Deposited in PMC for release after 12 months.

### Peer review history

The peer review history is available online at <https://journals.biologists.com/dev/article-lookup/doi/10.1242/dev.200355>.

### References

- Aponte-Santiago, N. A., Ormerod, K. G., Akbergenova, Y. and Littleton, J. T. (2020). Synaptic plasticity induced by differential manipulation of tonic and phasic motoneurons in *Drosophila*. *J. Neurosci.* **40**, 6270–6288. doi:10.1523/JNEUROSCI.0925-20.2020
- Ashley, J., Sorrentino, V., Lobb-Rabe, M., Nagarkar-Jaiswal, S., Tan, L., Xu, S., Xiao, Q., Zinn, K. and Carrillo, R. A. (2019). Transsynaptic interactions between IgSF proteins DIP- $\alpha$  and Dpr10 are required for motor neuron targeting specificity. *eLife* **8**, e42690. doi:10.7554/eLife.42690
- Bali, N., Lee, H.-K. P. and Zinn, K. (2022). Sticks and stones, a conserved cell surface ligand for the Type IIa RPTP Lar, regulates neural circuit wiring in *Drosophila*. *Elife* **11**, e71469. doi:10.7554/eLife.71469
- Barish, S., Nuss, S., Strunilin, I., Bao, S., Mukherjee, S., Jones, C. D. and Volkan, P. C. (2018). Combinations of DIPs and Dprs control organization of olfactory receptor neuron terminals in *Drosophila*. *PLoS Genet.* **14**, e1007560. doi:10.1371/journal.pgen.1007560
- Bataillé, L., Frenedo, J.-L. and Vincent, A. (2015). Hox control of *Drosophila* larval anatomy; the alary and thoracic alary-related muscles. *Mech. Dev.* **138**, 170–176. doi:10.1016/j.mod.2015.07.005
- Bate, M. (1990). The embryonic development of larval muscles in *Drosophila*. *Dev. Camb. Engl.* **110**, 791–804. doi:10.1242/dev.110.3.791
- Bittern, J., Pogodalla, N., Ohm, H., Brüser, L., Kottmeier, R., Schirmeier, S. and Klämbt, C. (2020). Neuron–Glia Interaction in the *Drosophila* nervous system. *Dev. Neurobiol.* **81**, 438–452. doi:10.1002/dneu.22737
- Bornstein, B., Meltzer, H., Adler, R., Alyagor, I., Berkun, V., Cummings, G., Reh, F., Keren-Shaul, H., David, E., Riemensperger, T. et al. (2021). Transneuronal Dpr12/DIP- $\delta$  interactions facilitate compartmentalized dopaminergic innervation of *Drosophila* mushroom body axons. *EMBO J.* **40**, e105763. doi:10.15252/emboj.2020105763
- Broadus, J., Skeath, J. B., Spana, E. P., Bossing, T., Technau, G. and Doe, C. Q. (1995). New neuroblast markers and the origin of the aCC/pCC neurons in the *Drosophila* central nervous system. *Mech. Dev.* **53**, 393–402. doi:10.1016/0925-4773(95)00454-8
- Brovero, S. G., Fortier, J. C., Hu, H., Lovejoy, P. C., Newell, N. R., Palmateer, C. M., Tzeng, R.-Y., Lee, P.-T., Zinn, K. and Arbeitman, M. N. (2021). Investigation of *Drosophila* fruitless neurons that express Dpr/DIP cell adhesion molecules. *Elife* **10**, e63101. doi:10.7554/eLife.63101
- Carrillo, R. A., Özkan, E., Menon, K. P., Nagarkar-Jaiswal, S., Lee, P.-T., Jeon, M., Birnbaum, M. E., Bellen, H. J., Garcia, K. C. and Zinn, K. (2015). Control of synaptic connectivity by a network of *Drosophila* IgSF cell surface proteins. *Cell* **163**, 1770–1782. doi:10.1016/j.cell.2015.11.022
- Cheng, S., Park, Y., Kurleto, J. D., Jeon, M., Zinn, K., Thornton, J. W. and Özkan, E. (2019). Family of neural wiring receptors in bilaterians defined by



- phylogenetic, biochemical, and structural evidence. *Proc. Natl. Acad. Sci. USA* **116**, 201818631. doi:10.1073/pnas.1818631116
- Chiba, A., Snow, P., Keshishian, H. and Hotta, Y.** (1995). Fasciclin III as a synaptic target recognition molecule in *Drosophila*. *Nature* **374**, 166-168. doi:10.1038/374166a0
- Choi, J. C., Park, D. and Griffith, L. C.** (2004). Electrophysiological and morphological characterization of identified motor neurons in the *Drosophila* third instar larva central nervous system. *J. Neurophysiol.* **91**, 2353-2365. doi:10.1152/jn.01115.2003
- Cosmanescu, F., Katsamba, P. S., Sergeeva, A. P., Ahlsen, G., Patel, S. D., Brewer, J. J., Tan, L., Xu, S., Xiao, Q., Nagarkar-Jaiswal, S. et al.** (2018). Neuron-subtype-specific expression, interaction affinities, and specificity determinants of DIP/Dpr cell recognition proteins. *Neuron* **100**, 1385-1400.e6. doi:10.1016/j.neuron.2018.10.046
- Courgeon, M. and Desplan, C.** (2019). Coordination between stochastic and deterministic specification in the *Drosophila* visual system. *Science* **366**, eaay6727. doi:10.1126/science.aay6727
- Davis, G. W., Schuster, C. M. and Goodman, C. S.** (1997). Genetic analysis of the mechanisms controlling target selection: target-derived fasciclin II regulates the pattern of synapse formation. *Neuron* **19**, 561-573. doi:10.1016/S0896-6273(00)80372-4
- Diao, F., Ironfield, H., Luan, H., Diao, F., Shropshire, W. C., Ewer, J., Marr, E., Potter, C. J., Landgraf, M. and White, B. H.** (2015). Plug-and-play genetic access to *Drosophila* cell types using exchangeable exon cassettes. *Cell Rep.* **10**, 1410-1421. doi:10.1016/j.celrep.2015.01.059
- Doe, C. Q., Smouse, D. and Goodman, C. S.** (1988). Control of neuronal fate by the *Drosophila* segmentation gene even-skipped. *Nature* **333**, 376-378. doi:10.1038/333376a0
- Estacio-Gómez, A. and Díaz-Benjumea, F. J.** (2013). Roles of Hox genes in the patterning of the central nervous system of *Drosophila*. *Fly* **8**, 26-32. doi:10.4161/fly.27424
- Evans, C. J., Olson, J. M., Ngo, K. T., Kim, E., Lee, N. E., Kuoy, E., Patananan, A. N., Sitz, D., Tran, P., Do, M.-T. et al.** (2009). G-TRACE: rapid Gal4-based cell lineage analysis in *Drosophila*. *Nat. Methods* **6**, 603-605. doi:10.1038/nmeth.1356
- Gorczyca, M. G., Phillis, R. W. and Budnik, V.** (1994). The role of tinman, a mesodermal cell fate gene, in axon pathfinding during the development of the transverse nerve in *Drosophila*. *Development* **120**, 2143-2152. doi:10.1242/dev.120.8.2143
- Grueber, W. B., Jan, L. Y. and Jan, Y. N.** (2002). Tiling of the *Drosophila* epidermis by multidendritic sensory neurons. *Development* **129**, 2867-2878. doi:10.1242/dev.129.12.2867
- Grueber, W. B., Ye, B., Yang, C.-H., Younger, S., Borden, K., Jan, L. Y. and Jan, Y.-N.** (2007). Projections of *Drosophila* multidendritic neurons in the central nervous system: links with peripheral dendrite morphology. *Development* **134**, 55-64. doi:10.1242/dev.02666
- Hattori, D., Chen, Y., Matthews, B. J., Salwinski, L., Sabatti, C., Grueber, W. B. and Zipursky, S. L.** (2009). Robust discrimination between self and non-self neurites requires thousands of Dscam1 isoforms. *Nature* **461**, 644-648. doi:10.1038/nature08431
- Heckscher, E. S., Zarin, A. A., Faumont, S., Clark, M. Q., Manning, L., Fushiki, A., Schneider-Mizell, C. M., Fetter, R. D., Truman, J. W., Zwart, M. F. et al.** (2015). Even-Skipped+ interneurons are core components of a sensorimotor circuit that maintains left-right symmetric muscle contraction amplitude. *Neuron* **88**, 314-329. doi:10.1016/j.neuron.2015.09.009
- Hoang, B. and Chiba, A.** (2001). Single-cell analysis of *Drosophila* larval neuromuscular synapses. *Dev. Biol.* **229**, 55-70. doi:10.1006/dbio.2000.9983
- Hong, W., Mosca, T. J. and Luo, L.** (2012). Teneurins instruct synaptic partner matching in an olfactory map. *Nature* **484**, 201-207. doi:10.1038/nature10926
- Honig, B. and Shapiro, L.** (2020). Adhesion protein structure, molecular affinities, and principles of cell-cell recognition. *Cell* **181**, 520-535. doi:10.1016/j.cell.2020.04.010
- Hooper, J. E.** (1986). Homeotic gene function in the muscles of *Drosophila* larvae. *EMBO J.* **5**, 2321-2329. doi:10.1002/j.1460-2075.1986.tb04500.x
- Inaki, M., Shinza-Kameda, M., Ismat, A., Frasch, M. and Nose, A.** (2010). *Drosophila* Tey represses transcription of the repulsive cue Toll and generates neuromuscular target specificity. *Development* **137**, 2139-2146. doi:10.1242/dev.046672
- Jan, L. Y. and Jan, Y. N.** (1982). Antibodies to horseradish peroxidase as specific neuronal markers in *Drosophila* and in grasshopper embryos. *Proc. Natl. Acad. Sci. USA* **79**, 2700-2704. doi:10.1073/pnas.79.8.2700
- Jontes, J. D.** (2017). The cadherin superfamily in neural circuit assembly. *Csh. Perspect Biol.* **10**, a029306. doi:10.1101/cshperspect.a029306
- Kanca, O., Zirin, J., Garcia-Marques, J., Knight, S. M., Yang-Zhou, D., Amador, G., Chung, H., Zuo, Z., Ma, L., He, Y. et al.** (2019). An efficient CRISPR-based strategy to insert small and large fragments of DNA using short homology arms. *Elife* **8**, e51539. doi:10.7554/eLife.51539
- Kim, M. D., Wen, Y. and Jan, Y.-N.** (2009). Patterning and organization of motor neuron dendrites in the *Drosophila* larva. *Dev. Biol.* **336**, 213-221. doi:10.1016/j.ydbio.2009.09.041
- Kose, H., Rose, D., Zhu, X. and Chiba, A.** (1997). Homophilic synaptic target recognition mediated by immunoglobulin-like cell adhesion molecule Fasciclin III. *Development* **124**, 4143-4152. doi:10.1242/dev.124.20.4143
- Kottmeier, R., Bittern, J., Schoofs, A., Scheiwe, F., Matzat, T., Pankratz, M. and Klämbt, C.** (2020). Wrapping glia regulates neuronal signaling speed and precision in the peripheral nervous system of *Drosophila*. *Nat. Commun.* **11**, 4491. doi:10.1038/s41467-020-18291-1
- Kurmangaliyev, Y. Z., Yoo, J., Valdes-Aleman, J., Sanfilippo, P. and Zipursky, S. L.** (2020). Transcriptional programs of circuit assembly in the *Drosophila* visual system. *Neuron* **108**, 1045-1057.e6. doi:10.1016/j.neuron.2020.10.006
- Kurusu, M., Cording, A., Taniguchi, M., Menon, K., Suzuki, E. and Zinn, K.** (2008). A screen of cell-surface molecules identifies leucine-rich repeat proteins as key mediators of synaptic target selection. *Neuron* **59**, 972-985. doi:10.1016/j.neuron.2008.07.037
- Landgraf, M. and Thor, S.** (2006). Development of *Drosophila* motoneurons: Specification and morphology. *Semin. Cell Dev. Biol.* **17**, 3-11. doi:10.1016/j.semcdb.2005.11.007
- Landgraf, M., Bossing, T., Technau, G. M. and Bate, M.** (1997). The origin, location, and projections of the embryonic abdominal motoneurons of *Drosophila*. *J. Neurosci.* **17**, 9642-9655. doi:10.1523/JNEUROSCI.17-24-09642.1997
- Landgraf, M., Sánchez-Soriano, N., Technau, G. M., Urban, J. and Prokop, A.** (2003a). Charting the *Drosophila* neuropile: a strategy for the standardized characterisation of genetically amenable neurites. *Dev. Biol.* **260**, 207-225. doi:10.1016/S0012-1606(03)00215-X
- Landgraf, M., Jeffrey, V., Fujioka, M., Jaynes, J. B. and Bate, M.** (2003b). Embryonic origins of a motor system: motor dendrites form a myotopic map in *Drosophila*. *PLoS Biol.* **1**, e41. doi:10.1371/journal.pbio.0000041
- Lee, P.-T., Zirin, J., Kanca, O., Lin, W.-W., Schulze, K. L., Li-Kroeger, D., Tao, R., Devereaux, C., Hu, Y., Chung, V. et al.** (2018). A gene-specific T2A-GAL4 library for *Drosophila*. *Elife* **7**, e35574. doi:10.7554/eLife.35574
- Li, H.** (2020). Single-cell RNA sequencing in *Drosophila*: technologies and applications. *Wiley Interdiscip Rev. Dev. Biol.* **10**, e396. doi:10.1002/wdev.396
- Li, H.-H., Kroll, J. R., Lennox, S. M., Ogundeyi, O., Jeter, J., Depasquale, G. and Truman, J. W.** (2014). A GAL4 driver resource for developmental and behavioral studies on the larval CNS of *Drosophila*. *Cell Rep.* **8**, 897-908. doi:10.1016/j.celrep.2014.06.065
- Lnenicka, G. A. and Keshishian, H.** (2000). Identified motor terminals in *Drosophila* larvae show distinct differences in morphology and physiology. *J. Neurobiol.* **43**, 186-197. doi:10.1002/(SICI)1097-4695(200005)43:2<186::AID-NEU8>3.0.CO;2-N
- Logan, J., Falck-Pedersen, E., Darnell, J. E. and Shenk, T.** (1987). A poly(A) addition site and a downstream termination region are required for efficient cessation of transcription by RNA polymerase II in the mouse beta maj-globin gene. *Proc. Natl. Acad. Sci. USA* **84**, 8306-8310. doi:10.1073/pnas.84.23.8306
- Ma, D., Przybylski, D., Abruzzi, K. C., Schlichting, M., Li, Q., Long, X. and Rosbash, M.** (2021). A transcriptomic taxonomy of *Drosophila* circadian neurons around the clock. *Elife* **10**, e63056. doi:10.7554/eLife.63056
- Macleod, G. T., Suster, M. L., Charlton, M. P. and Atwood, H. L.** (2003). Single neuron activity in the *Drosophila* larval CNS detected with calcium indicators. *J. Neurosci. Meth.* **127**, 167-178. doi:10.1016/S0165-0270(03)00127-4
- Mauss, A., Tripodi, M., Evers, J. F. and Landgraf, M.** (2009). Midline signalling systems direct the formation of a neural map by dendritic targeting in the *Drosophila* motor system. *PLoS Biol.* **7**, e1000200. doi:10.1371/journal.pbio.1000200
- Meltzer, S., Yadav, S., Lee, J., Soba, P., Younger, S. H., Jin, P., Zhang, W., Parrish, J., Jan, L. Y. and Jan, Y.-N.** (2016). Epidermis-derived semaphorin promotes dendrite self-avoidance by regulating dendrite-substrate adhesion in *Drosophila* sensory neurons. *Neuron* **89**, 741-755. doi:10.1016/j.neuron.2016.01.020
- Meng, J. L. and Heckscher, E. S.** (2020). Development of motor circuits: from neuronal stem cells and neuronal diversity to motor circuit assembly. *Curr. Top. Dev. Biol.* **142**, 409-442. doi:10.1016/bs.ctdb.2020.11.010
- Menon, K. P., Carrillo, R. A. and Zinn, K.** (2013). Development and plasticity of the *Drosophila* larval neuromuscular junction. *Wiley Interdiscip Rev. Dev. Biol.* **2**, 647-670. doi:10.1002/wdev.108
- Menon, K. P., Kulkarni, V., Takemura, S., Anaya, M. and Zinn, K.** (2019). Interactions between Dpr11 and DIP- $\gamma$  control selection of amacrine neurons in *Drosophila* color vision circuits. *Elife* **8**, e48935. doi:10.7554/eLife.48935
- Merritt, D. J. and Murphey, R. K.** (1992). Projections of leg proprioceptors within the CNS of the fly *Phormia* in relation to the generalized insect ganglion. *J. Comp. Neurol.* **322**, 16-34. doi:10.1002/cne.903220103
- Merritt, D. and Whittington, P.** (1995). Central projections of sensory neurons in the *Drosophila* embryo correlate with sensory modality, soma position, and proneural gene function. *J. Neurosci.* **15**, 1755-1767. doi:10.1523/JNEUROSCI.15-03-01755.1995
- Miura, S. K., Martins, A., Zhang, K. X., Graveley, B. R. and Zipursky, S. L.** (2013). Probabilistic splicing of Dscam1 establishes identity at the level of single neurons. *Cell* **155**, 1166-1177. doi:10.1016/j.cell.2013.10.018

- Murphey, R. K., Possidente, D., Pollack, G. and Merritt, D. J. (1989). Modality-specific axonal projections in the CNS of the flies *Phormia* and *Drosophila*. *J. Comp. Neurol.* **290**, 185-200. doi:10.1002/cne.902900203
- Nagarkar-Jaiswal, S., Lee, P.-T., Campbell, M. E., Chen, K., Anguiano-Zarate, S., Gutierrez, M. C., Busby, T., Lin, W.-W., He, Y., Schulze, K. L. et al. (2015a). A library of MiMICs allows tagging of genes and reversible, spatial and temporal knockdown of proteins in *Drosophila*. *Elife* **4**, e05338. doi:10.7554/eLife.05338
- Nagarkar-Jaiswal, S., DeLuca, S. Z., Lee, P.-T., Lin, W.-W., Pan, H., Zuo, Z., Lv, J., Spradling, A. C. and Bellen, H. J. (2015b). A genetic toolkit for tagging intronic MiMIC containing genes. *Elife* **4**, e08469. doi:10.7554/eLife.08469
- Nern, A., Pfeiffer, B. D. and Rubin, G. M. (2015). Optimized tools for multicolor stochastic labeling reveal diverse stereotyped cell arrangements in the fly visual system. *Proc. Natl. Acad. Sci. USA* **112**, E2967-E2976. doi:10.1073/pnas.1506763112
- Nguyen, T. H., Vicidomini, R., Choudhury, S. D., Coon, S. L., Iben, J., Brody, T. and Serpe, M. (2021). Single-cell RNA sequencing analysis of the *Drosophila* larval ventral cord. *Curr. Protoc.* **1**, e38. doi:10.1002/cpz1.38
- Nose, A. (2012). Generation of neuromuscular specificity in *Drosophila*: novel mechanisms revealed by new technologies. *Front Mol Neurosci* **5**, 62. doi:10.3389/fnmol.2012.00062
- Nose, A., Mahajan, V. B. and Goodman, C. S. (1992). Connectin: a homophilic cell adhesion molecule expressed on a subset of muscles and the motoneurons that innervate them in *Drosophila*. *Cell* **70**, 553-567. doi:10.1016/0092-8674(92)90426-D
- Nose, A., Umeda, T. and Takeichi, M. (1997). Neuromuscular target recognition by a homophilic interaction of connectin cell adhesion molecules in *Drosophila*. *Development* **124**, 1433-1441. doi:10.1242/dev.124.8.1433
- Orgogozo, V. and Grueber, W. B. (2005). FlyPNS, a database of the *Drosophila* embryonic and larval peripheral nervous system. *BMC Dev. Biol.* **5**, 4. doi:10.1186/1471-213X-5-4
- Özkan, E., Carrillo, R. A., Eastman, C. L., Weiszmann, R., Waghray, D., Johnson, K. G., Zinn, K., Celniker, S. E. and Garcia, K. C. (2013). An extracellular interactome of immunoglobulin and LRR proteins reveals receptor-ligand networks. *Cell* **154**, 228-239. doi:10.1016/j.cell.2013.06.006
- Pérez-Moreno, J. J. and O’Kane, C. J. (2018). GAL4 drivers specific for type Ib and type II motor neurons in *Drosophila*. *G3 (Bethesda)* **9**: 453-462. doi:10.1534/g3.118.200809
- Ponton, F., Chapuis, M.-P., Pernice, M., Sword, G. A. and Simpson, S. J. (2011). Evaluation of potential reference genes for reverse transcription-qPCR studies of physiological responses in *Drosophila melanogaster*. *J. Insect Physiol.* **57**, 840-850. doi:10.1016/j.jinsphys.2011.03.014
- Rose, D., Zhu, X., Kose, H., Hoang, B., Cho, J. and Chiba, A. (1997). Toll, a muscle cell surface molecule, locally inhibits synaptic initiation of the RP3 motoneuron growth cone in *Drosophila*. *Development* **124**, 1561-1571. doi:10.1242/dev.124.8.1561
- Sanes, J. R. and Zipursky, S. L. (2020). Synaptic specificity, recognition molecules, and assembly of neural circuits. *Cell* **181**, 536-556. doi:10.1016/j.cell.2020.04.008
- Schmid, A., Chiba, A. and Doe, C. Q. (1999). Clonal analysis of *Drosophila* embryonic neuroblasts: neural cell types, axon projections and muscle targets. *Development* **126**, 4653-4689. doi:10.1242/dev.126.21.4653
- Schrader, S. and Merritt, D. J. (2000). Central projections of *Drosophila* sensory neurons in the transition from embryo to larva. *J. Comp. Neurol.* **425**, 34-44. doi:10.1002/1096-9861(20000911)425:1<34::AID-CNE4>3.0.CO;2-G
- Shishido, E., Takeichi, M. and Nose, A. (1998). *Drosophila* synapse formation: regulation by transmembrane protein with leu-rich repeats, CAPRICIOUS. *Science* **280**, 2118-2121. doi:10.1126/science.280.5372.2118
- Simon, F. and Konstantinides, N. (2021). Single-cell transcriptomics in the *Drosophila* visual system: Advances and perspectives on cell identity regulation, connectivity, and neuronal diversity evolution. *Dev. Biol.* **479**, 107-122. doi:10.1016/j.ydbio.2021.08.001
- Sink, H. and Whittington, P. (1991a). Pathfinding in the central nervous system and periphery by identified embryonic *Drosophila* motor axons. *Development (Cambridge, England)* **112**, 307-316. doi:10.1242/dev.112.1.307
- Sink, H. and Whittington, P. M. (1991b). Location and connectivity of abdominal motoneurons in the embryo and larva of *Drosophila melanogaster*. *J. Neurobiol.* **22**, 298-311. doi:10.1002/neu.480220309
- Soba, P., Zhu, S., Emoto, K., Younger, S., Yang, S.-J., Yu, H.-H., Lee, T., Jan, L. Y. and Jan, Y.-N. (2007). *Drosophila* sensory neurons require dscam for dendritic self-avoidance and proper dendritic field organization. *Neuron* **54**, 403-416. doi:10.1016/j.neuron.2007.03.029
- Szymczak-Workman, A. L., Vignali, K. M. and Vignali, D. A. A. (2012). Design and construction of 2A peptide-linked multicistronic vectors. *Cold Spring Harb. Protoc.* **2012**, 199-204. doi:10.1101/pdb.ip067876
- Takizawa, E., Komatsu, A. and Tsujimura, H. (2007). Identification of common excitatory motoneurons in *Drosophila melanogaster* larvae. *Zool. Sci.* **24**, 504-513. doi:10.2108/zsj.24.504
- Tan, L., Zhang, K. X., Pecot, M. Y., Nagarkar-Jaiswal, S., Lee, P.-T., Takemura, S., McEwen, J. M., Nern, A., Xu, S., Tadros, W. et al. (2015). Ig superfamily ligand and receptor pairs expressed in synaptic partners in *Drosophila*. *Cell* **163**, 1756-1769. doi:10.1016/j.cell.2015.11.021
- Thor, S. and Thomas, J. B. (1997). The *Drosophila* islet gene governs axon pathfinding and neurotransmitter identity. *Neuron* **18**, 397-409. doi:10.1016/S0896-6273(00)81241-6
- Valdes-Aleman, J., Fetter, R. D., Sales, E. C., Heckman, E. L., Venkatasubramanian, L., Doe, C. Q., Landgraf, M., Cardona, A. and Zlatic, M. (2021). Comparative connectomics reveals how partner identity, location, and activity specify synaptic connectivity in *Drosophila*. *Neuron* **109**, 105-122.e7. doi:10.1016/j.neuron.2020.10.004
- Veling, M. W., Li, Y., Veling, M. T., Litts, C., Michki, N., Liu, H., Ye, B. and Cai, D. (2019). Identification of neuronal lineages in the *Drosophila* peripheral nervous system with a “Digital” multi-spectral lineage tracing system. *Cell Rep.* **29**, 3303-3312.e3. doi:10.1016/j.celrep.2019.10.124
- Venkatasubramanian, L., Guo, Z., Xu, S., Tan, L., Xiao, Q., Nagarkar-Jaiswal, S. and Mann, R. S. (2019). Stereotyped terminal axon branching of leg motor neurons mediated by IgSF proteins DIP- $\alpha$  and Dpr10. *Elife* **8**, e42692. doi:10.7554/eLife.42692
- Venken, K. J. T., Schulze, K. L., Haelterman, N. A., Pan, H., He, Y., Evans-Holm, M., Carlson, J. W., Levis, R. W., Spradling, A. C., Hoskins, R. A. et al. (2011). MiMIC: a highly versatile transposon insertion resource for engineering *Drosophila melanogaster* genes. *Nat. Methods* **8**, 737-743. doi:10.1038/nmeth.1662
- Vicidomini, R., Nguyen, T. H., Choudhury, S. D., Brody, T. and Serpe, M. (2021). Assembly and exploration of a single cell atlas of the *Drosophila* larval ventral cord. Identification of rare cell types. *Curr. Protoc.* **1**, e37. doi:10.1002/cpz1.37
- Wang, J., Ma, X., Yang, J. S., Zheng, X., Zugates, C. T., Lee, C.-H. J. and Lee, T. (2004). Transmembrane/juxtamembrane domain-dependent dscam distribution and function during mushroom body neuronal morphogenesis. *Neuron* **43**, 663-672. doi:10.1016/j.neuron.2004.06.033
- Wang, Y., Lobb-Rabe, M., Ashley, J., Anand, V. and Carrillo, R. A. (2021). Structural and functional synaptic plasticity induced by convergent synapse loss in the *Drosophila* neuromuscular circuit. *J. Neurosci.* **41**, 1401-1417. doi:10.1523/JNEUROSCI.1492-20.2020
- Winberg, M. L., Mitchell, K. J. and Goodman, C. S. (1998). Genetic analysis of the mechanisms controlling target selection: complementary and combinatorial functions of netrins, semaphorins, and IgCAMs. *Cell* **93**, 581-591. doi:10.1016/S0092-8674(00)81187-3
- de Wit, J., and Ghosh, A. (2016). Specification of synaptic connectivity by cell surface interactions. *Nat. Rev. Neurosci.* **17**, 4. doi:10.1038/nrn.2015.3
- Xie, Q., Brbic, M., Horns, F., Kolluru, S. S., Jones, R. C., Li, J., Reddy, A. R., Xie, A., Kohani, S., Li, Z. et al. (2021). Temporal evolution of single-cell transcriptomes of *Drosophila* olfactory projection neurons. *Elife* **10**, e63450. doi:10.7554/eLife.63450
- Xu, S., Xiao, Q., Cosmanescu, F., Sergeeva, A. P., Yoo, J., Lin, Y., Katsamba, P. S., Ahlsen, G., Kaufman, J., Linaval, N. T. et al. (2018). Interactions between the Ig-superfamily proteins DIP- $\alpha$  and Dpr6/10 regulate assembly of neural circuits. *Neuron* **100**, 1369-1384.e6. doi:10.1016/j.neuron.2018.11.001
- Xu, C., Theisen, E., Maloney, R., Peng, J., Santiago, I., Yapp, C., Werkhoven, Z., Rumbaut, E., Shum, B., Tarnogorska, D. et al. (2019). Control of synaptic specificity by establishing a relative preference for synaptic partners. *Neuron* **103**, 865-877.e7. doi:10.1016/j.neuron.2019.06.006
- Yildirim, K., Petri, J., Kottmeier, R. and Klämbt, C. (2019). *Drosophila* glia: few cell types and many conserved functions. *Glia* **67**, 5-26. doi:10.1002/glia.23459
- Yoshihara, M., Rheuben, M. B. and Kidokoro, Y. (1997). Transition from growth cone to functional motor nerve terminal in *Drosophila* embryos. *J. Neurosci.* **17**, 8408-8426. doi:10.1523/JNEUROSCI.17-21-08408.1997
- Zarin, A. A. and Labrador, J.-P. (2019). Motor axon guidance in *Drosophila*. *Semin. Cell Dev. Biol.* **85**, 36-47. doi:10.1016/j.semcdb.2017.11.013
- Zarin, A. A., Mark, B., Cardona, A., Litwin-Kumar, A. and Doe, C. Q. (2019). A multilayer circuit architecture for the generation of distinct locomotor behaviors in *Drosophila*. *Elife* **8**, e51781. doi:10.7554/eLife.51781
- Zhan, X.-L., Clemens, J. C., Neves, G., Hattori, D., Flanagan, J. J., Hummel, T., Vasconcelos, M. L., Chess, A. and Zipursky, S. L. (2004). Analysis of dscam diversity in regulating axon guidance in *Drosophila* mushroom bodies. *Neuron* **43**, 673-686. doi:10.1016/j.neuron.2004.07.020
- Zhang, H., Rigo, F. and Martinson, H. G. (2015). Poly(A) signal-dependent transcription termination occurs through a conformational change mechanism that does not require cleavage at the poly(A) site. *Mol. Cell* **59**, 437-448. doi:10.1016/j.molcel.2015.06.008
- Zinn, K. and Özkan, E. (2017). Neural immunoglobulin superfamily interaction networks. *Curr. Opin. Neurobiol.* **45**, 99-105. doi:10.1016/j.conb.2017.05.010